

# Tidal evolution of eccentric orbits in massive binary systems

## a study of resonance locking

M.G. Witte and G.J. Savonije

Astronomical Institute ‘Anton Pannekoek’, University of Amsterdam, Kruislaan 403, NL-1098 SJ Amsterdam, The Netherlands

Received 10 May 1999 / Accepted 6 July 1999

**Abstract.** We study the tidal evolution of a binary system consisting of a  $1.4 M_{\odot}$  compact object in elliptic orbit about a  $10 M_{\odot}$  uniformly rotating main sequence (MS) star for various values of the initial orbital parameters. We apply our previously published results of 2D non-adiabatic calculations of the non-radial g- and r-mode oscillations of the uniformly rotating MS star, and include the effects of resonant excitation of these modes in the tidal evolution calculations. A high orbital eccentricity enhances the effectiveness of the tidal interaction because of the large number of harmonic components of the tidal potential and the reduced orbital separation near periastron. By including the evolution of the MS star, especially of its rotation rate, many resonance crossings occur with enhanced tidal interaction. We analyse the phenomenon of resonance locking whereby a particular tidal harmonic is kept resonant with a stellar oscillation mode by the combined action of stellar evolution and other tidal harmonics. Resonance locking of prograde g-modes appears an effective mechanism for orbital circularization of eccentric orbits. We consider the orbital evolution of the binary pulsar PSR J0045-7319 and conclude that resonance locking could explain the observed short orbital decay time of this system if the B-star spins in the direction counter to the orbital motion.

**Key words:** stars: rotation – stars: oscillations – stars: binaries: close – hydrodynamics

### 1. Introduction

Two (or more) celestial bodies which orbit each other will experience periodic deformations due to the fluctuations of the mutually attracting gravitational fields. The tidally induced flows in these bodies are subject to dissipative processes, causing a phase lag to develop between the perturbing potential and the displaced material. The resulting torque changes the orbital parameters of the system, and usually acts to drive the system towards circularization of the orbit and corotation of the components. If a binary system is in such a tidally relaxed state, it is relatively simple to calculate the tidally induced static shape

of the components, the so-called equilibrium tide. However, in general the tidal deformation is time dependent and requires dynamical effects to be taken into account. Cowling (1941) noted that the tidal forces can excite gravity (g-) modes in the radiative layers of binary stars, the so-called dynamical tides. In case of a high mass early type star the stellar envelope is radiative and gravity modes can be excited for which significant damping occurs in a layer beneath the stellar surface, where the local thermal timescale is comparable to the period of oscillation. Zahn (1977) developed an asymptotic theory valid for low forcing frequencies where the radiative damping is severe and resonances with g-modes are smeared out. However, when the system is far from equilibrium, tidal forcing contains relatively high frequencies, so that resonances with relatively weakly damped low radial order g-modes are likely to occur. Zahn’s theory may predict tidal timescales orders of magnitude too small when the asymptotic low frequency conditions are not met.

In a series of papers Savonije & Papaloizou (1983; 1984) presented non-adiabatic linearised calculations for perturbed spherical stellar models, enabling the study of resonantly excited g-modes at different stages of evolution of the star. To include effects of stellar rotation on the oscillations, an implicit 2D hydrodynamics code has been developed (Savonije and Papaloizou, 1997) in which centrifugal distortion is discarded, but which fully accommodates the arising Coriolis forces in the rotating star. Due to the Coriolis force the response of a rotating star to a spherical harmonic perturbing force is itself not a simple spherical harmonic function, but may be numerically solved on a 2D  $(r, \vartheta)$  grid. Using the 2D-code, the effects of rotation on the stellar (g-)modes can be examined, while also it is possible to study the stellar quasi-toroidal r-modes (see Papaloizou and Pringle, 1978) in detail. In a previous paper (Witte and Savonije, 1999) (Paper I) we utilised the above mentioned 2D code to calculate the g- and r-mode spectra of a  $10 M_{\odot}$  stellar model with a central hydrogen abundance of forty percent rotating uniformly at speeds up to forty percent of breakup. In order to study effects of the star’s evolution, we extend the data of Paper I with some calculations for a  $X_c = 0.2$  stellar model, the results of which are listed in the appendix of this paper. The strength of the r-mode resonances, as given by the area of the peaks, becomes larger in a more rapidly rotating star. For rapid

Send offprint requests to: M.G. Witte

Correspondence to: marnix@astro.uva.nl

stellar rotation with  $\Omega_s = 0.4 \Omega_c$ , the strongest r-modes have peak areas comparable to g-modes with approximately 7–10 radial nodes. Additionally the long wavelength weakly damped r-mode resonances occur at quite low forcing frequencies in a region where the stellar g-modes are severely damped as a result of their short wavelength. If, therefore, a star is forced with strong harmonics that lie in this region, resonant excitation of r-modes can be expected to dominate the orbital evolution of the system.

The recent discovery (see Kaspi et al., 1994) of the binary radio pulsar PSR J0045-7319, which contains a B-star and a neutron star in a highly eccentric orbit, and for which radio pulsar timing has lead to a fairly accurate measurement of orbital precession and orbital decay (see also Sect. 4), triggered a number of publications in the field of dynamical tides in wide eccentric binary systems (e.g. Kumar and Goodman, 1996; Lai, 1997; Kumar and Quataert, 1998). These papers considered some aspects of nonlinear coupling of modes, effects of stellar rotation and enhanced dissipation due to differential rotation by means of various approximations. We will now investigate, by detailed calculations, the effects of resonances with stellar oscillation modes (in a uniformly rotating MS star) on the tidal evolution of eccentric massive binary systems and apply our results to PSR J0045-7319.

## 2. Basic equations

We consider a binary system consisting of a  $M_s = 10 M_\odot$  main sequence star and a  $M_p = 1.4 M_\odot$  compact (NS) companion in an eccentric orbit with eccentricity  $e$  and orbital period  $P_{\text{orb}}$ . Such a system could be easily produced during the supernova explosion following a period of mass transfer from the initially more massive primary to the rejuvenated MS object (van den Heuvel and Heise, 1972).

The energy and angular momentum (magnitude) of the eccentric orbit is given by

$$E_{\text{orb}} = -GM_p M_s / 2a \text{ and } H_{\text{orb}} = \frac{M_p M_s}{M_p + M_s} a^2 \omega \sqrt{1 - e^2}$$

where  $a$  is the semi-major axis and  $\omega = 2\pi/P_{\text{orb}}$  the mean angular velocity of the stars in their elliptic orbit. For simplicity we assume the stellar spin angular momentum vector  $\mathbf{H}_s$  to be aligned with the orbital angular momentum vector. In this paper, we will only consider secular tidal changes in the magnitude of the orbital energy and angular momentum, and ignore changes in the configuration of the orbit as given by precession of the axes (which vanishes as the axes are assumed parallel) or advance of periastron (apsidal motion).

### 2.1. The tidal potential

Due to the motion of the companion in its eccentric orbit, the  $10 M_\odot$  MS star is exposed to a changing external gravitational field. We can facilitate the analysis by subdividing the forcing potential into its harmonic components and evaluating the contribution of each term to the tidal process separately. Labelling

the companion's coordinates relative to the star with a prime, its perturbing potential is expanded as the real part of (e.g. Morse and Feshbach, 1952)

$$\Phi_T(r, \vartheta, \varphi, t) = -\frac{GM_p}{a} \sum_{l=0}^{\infty} \sum_{m=0}^l \epsilon_m \frac{(l-m)!}{(l+m)!} \left(\frac{r}{a}\right)^l P_l^m(\cos \vartheta) \left(\frac{a}{r'}\right)^{l+1} P_l^m(\cos \frac{\pi}{2}) e^{im(\varphi' - \varphi)}$$

where  $P_l^m(\cos \vartheta)$  denotes the associated Legendre polynomial and  $\epsilon_m = 1$  for  $m = 0$  and  $2$  for  $m > 0$ . We assume  $m \geq 0$  and characterise retrograde relative orbital motion by a negative forcing frequency  $\bar{\sigma} = \sigma - m\Omega_s$  in the stellar frame. Fourier expansion of the time dependent terms gives

$$\left(\frac{a}{r'}\right)^{l+1} e^{im(\varphi' - \varphi)} = \sum_{n=-\infty}^{\infty} h_n^{(l+1),m} e^{i(nM - m\varphi)}$$

where  $M = \omega t$  is the mean anomaly. The Fourier coefficients (often called ‘Hansen coefficients’ in this context) are given by

$$h_n^{(l+1),m} = \frac{1}{2\pi} \int_{-\pi}^{\pi} \left(\frac{a}{r'}\right)^{l+1} e^{i(m\varphi' - kM)} dM.$$

The relative elliptic orbit can be expressed in the parameters  $e$ ,  $p$  and  $\varphi'$  or in  $e$ ,  $a$  and the eccentric anomaly  $E$ :

$$r' = \frac{p}{1 + e \cos \varphi'} = a(1 - e \cos E).$$

The eccentric anomaly  $E$  is related to  $M$  and  $\varphi'$  through (e.g. Brouwer and Clemence, 1961)

$$E - e \sin E = M$$

and

$$\tan\left(\frac{\varphi'}{2}\right) = \sqrt{\frac{1+e}{1-e}} \tan\left(\frac{E}{2}\right).$$

By scaling the Hansen coefficients as

$$c_n^{lm} = \left(\frac{GM_p}{a^{l+1}}\right) \epsilon_m \frac{(l-m)!}{(l+m)!} P_l^m\left(\cos \frac{\pi}{2}\right) h_n^{(l+1),m}, \quad (1)$$

the companion's tidal potential can be expressed as

$$\Phi_T(r, \vartheta, \varphi, t) = -\sum_{l=2}^{\infty} \sum_{m=0}^l r^l P_l^m(\cos \vartheta) \sum_{n=-\infty}^{\infty} c_n^{lm} \cos(n\omega t - m\varphi), \quad (2)$$

i.e. each tidal spherical harmonic component  $(l, m)$  can be expressed as a series of harmonics  $n$ , representing circular orbits with angular frequency  $n\omega$ . In this paper we only consider the dominant tidal components with  $l = 2$  and  $m = 0$  or  $m = 2$ . The  $m = 1$  contribution vanishes for the aligned case studied here. Modes with  $m = 0$  have no  $\varphi$  dependence, therefore no angular momentum can be transferred via these oscillations, only energy exchange can take place. For these axisymmetric

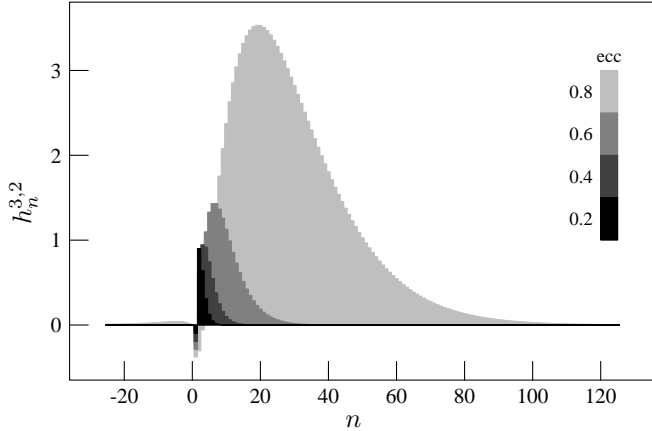


**Fig. 1.** Hansen coefficients  $h_n^{(l+1),m}$  with  $l = m = 2$  for eccentricities  $e = 0.2, 0.4, 0.6$  and  $0.8$ .

modes, the coefficients  $c_n^{lm} = c_{-n}^{lm}$ . For  $m = 2$  the coefficients with  $n < 0$  are negligible. In Fig. 1 we plot the Hansen coefficients for  $m = 2$  as a function of  $n$  for a few different values of the eccentricity. It is apparent that as the eccentricity increases, the number of contributing harmonics increases greatly, and also that the magnitude of the largest coefficients (which enters the expression for the torque quadratically) increases by a significant factor due to the diminishing orbital separation at periastron.

In our calculations we include  $n$ -values starting at  $n = 1$  and going up to  $n_{\max} = 2(m + l + 1)f_{\text{per}}$  to ensure that the companion's potential is accurately reproduced. For  $m = 0$  we take  $c_n^{lm}$  to be the sum of the positive and negative  $n$  contribution. Here,  $f_{\text{per}} = \sqrt{\frac{1+e}{(1-e)^3}}$  is the ratio between the orbital frequency in periastron  $\omega_{\text{per}}$  and the mean orbital frequency  $\omega$ .

## 2.2. Orbital evolution by the tidal exchange of energy and angular momentum

Situated in an eccentric orbit with its companion, the  $10 M_{\odot}$  star is simultaneously forced at many harmonic frequencies  $\bar{\sigma}_n = n\omega - m\Omega_s$  (in the stellar frame), the magnitude of each term being proportional to  $c_n^{lm}$ . The harmonic components with  $n < n_0 = m \text{int}(\Omega_s/\omega)$  correspond to negative forcing frequencies which means that the corresponding frequency in the inertial frame is smaller than the stellar rotation frequency. Hence in the stellar frame these components excite oscillations which run backwards. Excitation of such retrograde modes gives rise to spin-down of the star, while excitation of prograde modes ( $n > n_0$ ) has the opposite effect. This opens the possibility of simultaneous tidal interaction with counteracting resonances with prograde (spin-up) and retrograde (spin-down) oscillation modes. By assuming the response of the star to the tidal forcing can be approximated by a linear treatment the problem simplifies considerably since we may apply the superposition principle and decompose the stellar response into independent harmonic components. We further assume the stellar response to each harmonic has reached

a steady state in which the tidal excitation is balanced by radiative and viscous damping in the oscillating star. These approximations may break down during resonance passages although a steady state is usually a fairly good approximation, see discussion in Sect. 5. The steady state assumption allows us to calculate the stellar response as a strictly periodic phenomenon, i.e. we are not forced to follow the stellar oscillations on a dynamical timescale, which, at the current level and for the duration required to study secular evolution, would not be possible with present day computer facilities. The steady state tidal torque can be determined by applying the implicit 2D code mentioned above whereby the periodic term can be factored out. In Paper I we have shown that for each harmonic  $(l, m, n)$  in the forcing potential the work done by the tide (per time unit) on the star and the associated rate of change of spin angular momentum  $H_s$  can be expressed as:

$$\dot{E}_n^{lm} = \sigma_n \mathcal{T}_n^{lm} \quad \text{and} \quad \dot{H}_n^{lm} = m \mathcal{T}_n^{lm} \quad (3)$$

whereby the torque integral is defined as

$$\mathcal{T}_n^{lm} = -\pi c_n^{lm} \int_0^{R_s} \int_0^\pi \text{Im}(\rho'(r, \vartheta)) P_l^m(\cos \vartheta) r^{l+2} \sin \vartheta \, d\vartheta \, dr \quad (4)$$

where  $\text{Im}$  stands for imaginary part and  $P_l^m(\cos \vartheta)$  is the associated Legendre polynomial of index  $m$  and degree  $l$ . In steady state  $\dot{E}_n^{lm}$  equals the energy dissipation rate due to the  $n^{\text{th}}$  harmonic of the tidal  $(l, m)$  forcing. For a given forcing frequency  $\sigma_n = n\omega$  (in the inertial frame) the tidal perturbation of the stellar mass density  $\rho'(r, \vartheta)$  occurring in the above integral follows from the tidal response calculations in Paper I, see current appendix. Conservation of energy and angular momentum then implies that the rate of change of orbital energy and angular momentum follows by adding up the stellar rates of change in response to each harmonic term in the tidal potential and then reversing the sign:

$$\dot{E}_{\text{orb}} = - \sum_{l,m} \sum_n \dot{E}_n^{lm} \quad \text{and} \quad \dot{H}_{\text{orb}} = - \sum_{l,m} \sum_n \dot{H}_n^{lm}. \quad (5)$$

By expressing the orbital eccentricity  $e$  in terms of the stellar masses and the orbital energy  $E_{\text{orb}}$  and angular momentum  $H_{\text{orb}}$  (e.g. Landau and Lifshitz, 1959)

$$e = \sqrt{1 + \frac{2M_{\text{tot}}}{G^2 M_p^3 M_s^3} E_{\text{orb}} H_{\text{orb}}^2}$$

with  $M_{\text{tot}} = M_p + M_s$ , we can express the rate of change of the orbital eccentricity as

$$\frac{de^2}{dt} = \left( \frac{GM_p M_s}{2a} \right)^{-1} \left[ (1 - e^2) \dot{E}_{\text{orb}} - \omega \sqrt{1 - e^2} \dot{H}_{\text{orb}} \right] \quad (6)$$

We use this expression for the rate of change of the eccentricity to prevent numerical roundoff errors from producing negative eccentricities or generating eccentricity in a circular orbit. Finally, the rate of change of the semi-major axis follows from

$$\frac{1}{a} \frac{da}{dt} = \left( \frac{GM_p M_s}{2a} \right)^{-1} \dot{E}_{\text{orb}}. \quad (7)$$

By defining the eccentric orbit for given (fixed) stellar masses through  $a$  and  $e$  the tidal evolution of the orbit can be followed by numerically integrating Eqs. (6)–(7) whereby at every timestep the tidal exchange rates  $\dot{E}_{\text{orb}}$  and  $\dot{H}_{\text{orb}}$  are determined through Eqs. (3)–(5).

To investigate the resonant exchange of energy and angular momentum in detail, we developed a routine that enables us to calculate this tidal evolution by interpolating the tidal torque integral (4), as a function of forcing frequency  $\sigma_n$ , stellar spin rate  $\Omega_s$  and evolutionary state of the MS star (expressed in terms of the core hydrogen abundance  $X_c$ ) in the data presented in Paper I and Tables B1 and B2 (see appendix for more details).

### 2.3. Resonant exchange of energy and angular momentum

We have seen that in an eccentric binary system the tidal forcing of the star by its orbiting companion occurs in a non-harmonic time dependent manner. Decomposition of the forcing potential into harmonic components introduces a range of frequencies at which different harmonic modes of oscillation in the star are excited simultaneously. These forcing frequencies change as orbital evolution progresses due to the fact that the orbit may shrink or widen, and due to changes in the stellar rotation frequency. Moreover, as the system evolves, the stellar oscillation spectrum itself changes due to restructuring of the star in response to stellar evolution and due to spin-up or spin-down of the star caused by tidal effects and the changing stellar moment of inertia. These stellar changes result in shifting of the eigenfrequencies of the stellar modes on the nuclear timescale of the star (which becomes relatively short, with the possibility of rapid tidal evolution, near the end of core hydrogen burning (Savonije and Papaloizou, 1984)). Hence, as the orbit evolves, the forcing frequencies shift through the stellar oscillation spectrum, picking up resonances in the star as eigen frequencies are crossed. During a resonance passage, the rate at which energy and angular momentum exchange takes place between the star and the orbit (i.e. the companion) can be many orders of magnitude larger than in the non-resonant case. The total amount of exchanged angular momentum is obtained by integrating the torque over time; since the speed at which the forcing frequencies shift through the stellar oscillation spectrum will generally be proportional to the torque, a relatively large peak area in the torque–frequency graph does not guarantee a large relative contribution to the tidal evolution process. The angular momentum exchange by a resonance passage of the  $n^{\text{th}}$  harmonic component crossing resonance peak  $k$  can be expressed as:

$$(\Delta H)_{\text{res}} = \int m \mathcal{T}_n^{lm} dt = \int \frac{m \mathcal{T}_n^{lm}}{\frac{d(\bar{\sigma}_n - \bar{\sigma}_{0,k})}{dt}} d(\bar{\sigma}_n - \bar{\sigma}_{0,k}) \quad (8)$$

with  $\mathcal{T}_n^{lm}$  the torque integral (4). The rate at which a certain harmonic component  $n$  moves through the resonance with mode  $k$  (at frequency  $\bar{\sigma}_{0,k}$  in the stellar frame) is a function of the rate of change of the mean orbital and stellar angular speed

and the rate of stellar evolution (characterised by the rate of hydrogen depletion in the stellar core  $\dot{X}_c$ ):

$$\frac{d(\bar{\sigma}_n - \bar{\sigma}_{0,k})}{dt} = n \frac{d\omega}{dt} - m \frac{d\Omega_s}{dt} - \frac{\partial \bar{\sigma}_{0,k}}{\partial X_c} \frac{dX_c}{dt} - \frac{\partial \bar{\sigma}_{0,k}}{\partial \Omega_s} \frac{d\Omega_s}{dt}.$$

After separating the dynamical and the stellar evolution component we obtain

$$\begin{aligned} \frac{d(\bar{\sigma}_n - \bar{\sigma}_{0,k})}{dt} = n \frac{d\omega}{dt} - \frac{1}{I_s} \left( m + \frac{\partial \bar{\sigma}_{0,k}}{\partial \Omega_s} \right) \frac{dH_s}{dt} + \\ \left[ \frac{\Omega_s}{I_s} \left( m + \frac{\partial \bar{\sigma}_{0,k}}{\partial \Omega_s} \right) \frac{dI_s}{dX_c} - \frac{\partial \bar{\sigma}_{0,k}}{\partial X_c} \right] \frac{dX_c}{dt}, \end{aligned} \quad (9)$$

with  $I_s$  the stellar moment of inertia. We note that, while the second term on the right of Eq. (9) is proportional to  $\dot{H}_{\text{orb}}$ , the first term is, for given harmonic  $n$ , fully determined by  $\dot{E}_{\text{orb}}$ . Of course the last term is determined by stellar evolution.

### 2.4. Resonance locking

When a harmonic term  $n$  of the tidal potential comes into resonance with a stellar oscillation mode the resulting exchange of energy and angular momentum between the MS star and its companion usually leads to a rapid shift through the resonance, so that the resonance condition is quickly lost and the tidal exchange is rather limited. However, under special circumstances, the resonance condition may be sustained for a relatively long period of time. A necessary condition for such locking on to a resonance is that the right hand side of Eq. (9) attains a small value during resonance passage while, in order to drive a significant orbital evolution, the acting torque should be large. Substituting (3) and introducing the orbital moment of inertia  $I_{\text{orb}} = \frac{M_p M_s}{M_p + M_s} a^2$ , Eq. (9) can be expressed as:

$$\frac{d(\bar{\sigma}_n - \bar{\sigma}_{0,k})}{dt} = \epsilon \dot{X}_c + \sum_j \zeta_{nj} \mathcal{T}_j^{lm} \quad (10)$$

where  $l = m = 2$  (the  $m = 0$  contribution is usually negligible). The dynamical factor is defined as

$$\zeta_{nj} = \left[ \frac{3nj}{I_{\text{orb}}} - \frac{m}{I_s} \left( m + \frac{\partial \bar{\sigma}_{0,k}}{\partial \Omega_s} \right) \right]$$

while the stellar evolution factor is

$$\epsilon = \left[ \frac{\Omega_s}{I_s} \left( m + \frac{\partial \bar{\sigma}_{0,k}}{\partial \Omega_s} \right) \frac{dI_s}{dX_c} - \frac{\partial \bar{\sigma}_{0,k}}{\partial X_c} \right].$$

Typically  $\left| \frac{\partial \bar{\sigma}_{0,k}}{\partial \Omega_s} \right| \approx 0.5 < m$  for  $m = 2$  locking. For the orbits we will consider  $I_{\text{orb}}$  is typically two or three orders of magnitude larger than  $I_s$ . For sufficiently large values of  $n$  the diagonal factor  $\zeta = \zeta_{nn}$ , which governs the frequency shift relative to the resonance peak due to the action of the  $n^{\text{th}}$  harmonic itself, attains a small value. A harmonic term in the forcing potential which has a small self-shifting coefficient  $\zeta$  must be driven deep into a resonance before its influence on the frequency shifting becomes prominent. If its self-shifting tendency draws itself through the resonance, the small value

of  $\zeta$  results in a relatively slow resonance crossing with correspondingly enhanced exchange of energy and angular momentum. However, if the self-shift works in the direction opposite to the resonance crossing, the frequency shift (due to the combined action of the other harmonics and the effect of stellar evolution) towards the resonance peak may be halted, resulting in a locked condition. This locked condition, whereby the self-shift balances the effect of all other harmonics, may last for a long period, therefore the total effect on the orbit can be significant. The most efficient locking will occur when  $\zeta \simeq 0$ , i.e. for the tidal harmonic  $n \simeq n_\zeta \simeq m \text{int} \sqrt{\frac{I_{\text{orb}}}{3I_s}}$ , which depends on the system's orbital period. The locking condition depends on the distribution of the Hansen coefficients, i.e. on the orbital eccentricity and on the location of the stellar oscillation spectrum relative to the locked mode (on where the strongest modes are situated in frequency space).

Consider the common case where the  $n^{\text{th}}$  harmonic  $\bar{\sigma}_n$  approaches a resonance  $\bar{\sigma}_{0,k}$  from below, i.e.  $\bar{\sigma}_n - \bar{\sigma}_{0,k} < 0$  whereby  $\zeta = \zeta_{nn}$  is slightly negative. Assuming a MS star with prograde spin and  $n_\zeta > n_0 = m \text{int}(\Omega_s/\omega)$ , where  $n_0$  denotes the division between retrograde and prograde harmonics, we can define

$$S_1 = \sum_{1 \leq j \leq n_0} \zeta_{nj} \mathcal{T}_j^{lm} > 0$$

$$S_2 = \sum_{n_0 < j < n} \zeta_{nj} \mathcal{T}_j^{lm} < 0$$

$$S_3 = \sum_{j > n} \zeta_{nj} \mathcal{T}_j^{lm} > 0.$$

Note that all harmonics with  $j < n$  have  $\zeta_{nj} < 0$ , while all higher harmonics have  $\zeta_{nj} > 0$ , while the torque integrals  $\mathcal{T}_j^{lm} < 0$  for  $n < n_0$  and positive for  $n > n_0$ . Since  $\zeta < 0$  (but almost zero) the  $n^{\text{th}}$  harmonic tends to move away from the resonance at  $\bar{\sigma}_{0,k}$  and must be driven into resonance by the combined action of the other harmonics (which will interact with other resonances) and the weak (positive) effect of stellar evolution:

$$-\zeta \mathcal{T}_n^{lm} < S_1 + S_2 + S_3 + \epsilon \dot{X}_c.$$

Locking requires that, when driven deep into resonance, the  $n^{\text{th}}$  harmonic begins to dominate all other effects, so that its action can prevent resonance passage:

$$-\zeta \max(\mathcal{T}_n^{lm}) > S_1 + S_2 + S_3 + \epsilon \dot{X}_c. \quad (11)$$

The criterion is easily modified for a retrograde stellar spin or for  $n > n_0$ . We will meet several cases of resonance locking in the numerical results discussed below.

### 3. Results for moderately wide binary systems

From now on we express all frequencies in units of  $\Omega_c$  and note that we consider only the strongest tidal components of the companion's potential, i.e. the component for which  $l = 2$

with either  $m = 0$  or  $m = 2$ . Unless specifically stated, the initial evolution state of the MS star corresponds to a central hydrogen abundance  $X_c = 0.4$ .

Before we go on to the discussion of our numerical results, let us first express the rate of change of the orbital eccentricity (6) due to the action of a single resonance, by substituting the corresponding expressions (3) for  $\dot{E}_n^{lm}$  and  $\dot{H}_n^{lm}$  as:

$$\frac{de^2}{dt} = \left[ \frac{\omega \sqrt{1-e^2}}{E_{\text{orb}}} \right] \left( n \sqrt{1-e^2} - m \right) \mathcal{T}_n^{lm} \quad (12)$$

where the factor in square brackets is always negative. It follows that prograde harmonics ( $n > n_0$ ) would require  $n < m/\sqrt{1-e^2}$  to yield a resonant increase of the orbital eccentricity. Unless the eccentricity is unrealistically large these two conditions are mutually exclusive, so that resonances with prograde modes tend to decrease the orbital eccentricity. On the other hand, retrograde modes which have  $n < n_0$  and  $\mathcal{T}_n^{lm} < 0$  require  $n > m/\sqrt{1-e^2}$  to enlarge the orbital eccentricity. Depending on the stellar rotation rate these two conditions can possibly be fulfilled, so that resonances with retrograde  $m = 2$  modes may enlarge the orbital eccentricity. Given the large number of harmonics that appear in orbits with high eccentricities (of the order  $10^2$  for  $e \sim 0.8$ ), the orbital evolution of such binary systems can be quite complicated. However, before we study the high eccentricity case, we will first consider the simple case of an almost circular orbit to gain some insight in the effect of resonances.

#### 3.1. Case of a narrow, almost circular orbit

First, we illustrate how the inclusion of resonant effects influences the tidal evolution in case of an almost circular orbit, so that we have to deal with only few harmonics. This we do by evolving a fairly narrow orbit ( $P_{\text{orb}} = 3$  days) with eccentricity  $e = 0.02$  and a slowly rotating stellar component ( $P_s = 25$  days) until corotation and circularization is established, see Fig. 2. In Fig. 2e we depict the initial location (frequency) of the stellar  $l = m = 2$  modes in terms of the order  $n$  of the forcing harmonic and indicate which harmonics have the largest Hansen coefficients for this orbit. The  $m = 0$  modes play generally no prominent role in the evolution. For these low eccentricities ( $e^2 \ll 1$ ), we can use a low order expansion of the potential of the orbiting companion in powers of the eccentricity to analyse our numerical results. To first order in  $e$  the Hansen coefficients can be expressed as  $h_1^{3,0} = 3e$ ,  $h_1^{3,2} = -\frac{1}{2}e$ ,  $h_2^{3,2} = 1$  and  $h_3^{3,2} = \frac{7}{2}e$ , yielding for the tidal potential

$$\begin{aligned} \Phi_T(r, \vartheta, \varphi, t) = & -\frac{GM_P}{4a} \left( \frac{r}{a} \right)^2 \left( -6eP_2(\cos \vartheta) \cos \omega t \right. \\ & -\frac{1}{2}eP_2^2(\cos \vartheta) \cos(\omega t - 2\varphi) \\ & +P_2^2(\cos \vartheta) \cos(2\omega t - 2\varphi) \\ & \left. +\frac{7}{2}eP_2^2(\cos \vartheta) \cos(3\omega t - 2\varphi) \right) + O(e^2). \end{aligned} \quad (13)$$

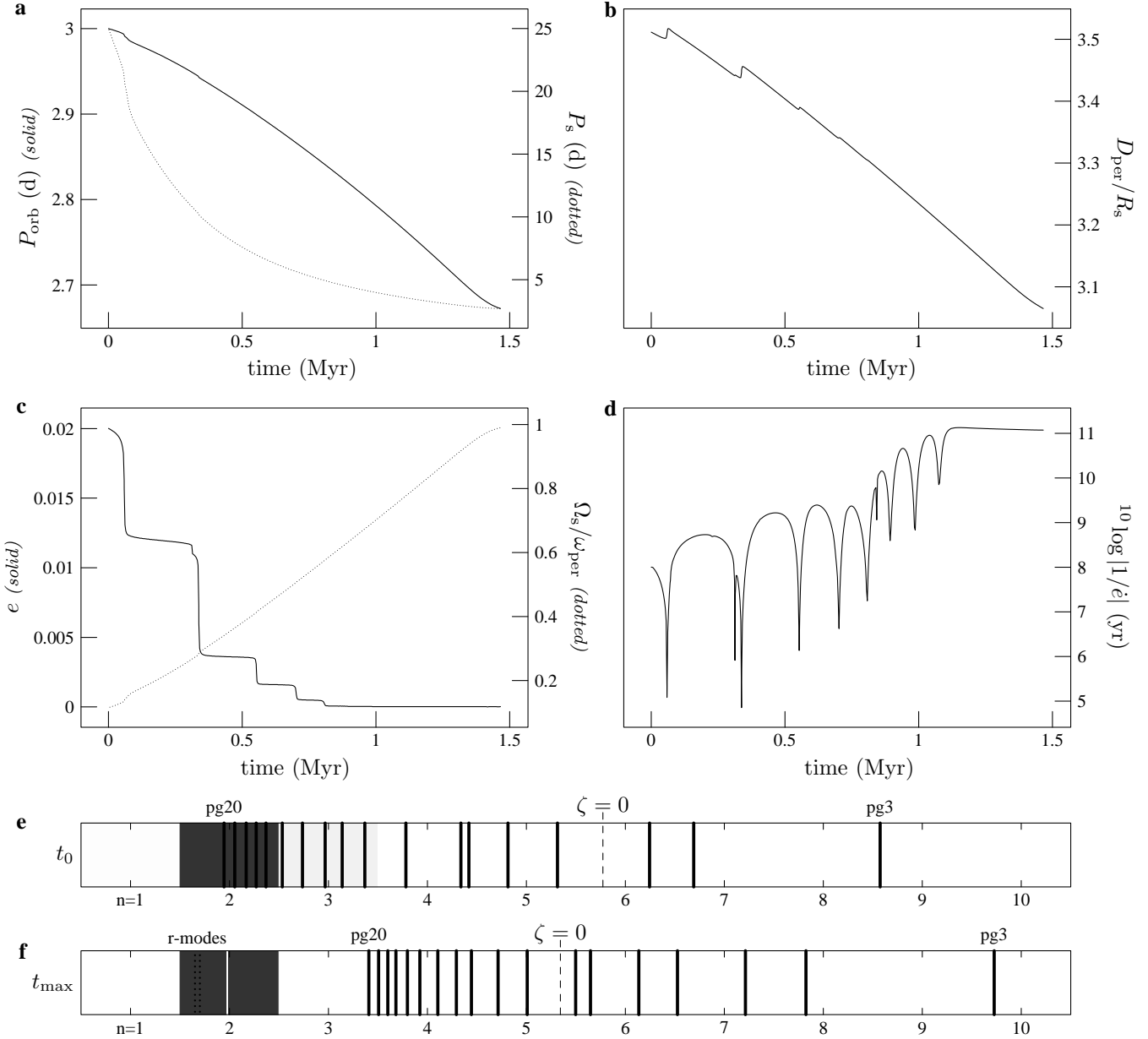


**Fig. 2.** Orbital evolution of a weakly eccentric ( $e = 0.02$ ) binary system which initially, at  $t = 0$ , harbours a slowly rotating MS star ( $P_s = 25$  days) in an orbit with a period of three days. During tidal evolution, resonant interaction through the  $n = 3$  harmonic decreases the eccentricity to very low values ( $e = 0.00012$  at  $t = 1.5$  Myr), while non-resonant interaction via the  $n = 2$  component forces the star into corotation. **a** Orbital (solid, left ordinate) and stellar (dotted, right ordinate) rotation period, **b** ratio of periastron distance to stellar radius, **c** eccentricity (solid, left ordinate) and ratio of stellar rotation frequency to orbital frequency at periastron (dotted, right ordinate), **d** timescale for the change of the eccentricity, **e** and **f** schematic representation of the frequency distribution of forcing harmonics and stellar resonance frequencies at  $t = 0$  (panel **e**) and  $t = t_{\text{max}}$  (panel **f**). Here, frequency increases from left to right, the contributing harmonic potentials have been labelled  $n = 1$  to  $10$  ( $= n_{\text{max}}$ ) and the gray level of each cell centred on  $n$  reflects the magnitude of the corresponding Hansen coefficient  $h_n^{3,2}$ . Due to the very low eccentricities only the cell with  $n = 2$  (and for  $t = 0$ , very vaguely,  $n = 3$ ) is printed gray. The frequencies of the stellar g-modes are given by thick lines, while the location of the r-modes is in between the dotted lines. In panel **e**, the r-modes are outside the range of the forcing harmonics and do not show up. The dashed line gives the frequency for which  $\zeta \equiv \zeta_{nn} = 0$  (see Eq. (10)). The white line (panel **f**) indicates the position where  $\bar{\sigma} = 0$ .

Note that the sign of the Hansen coefficients is irrelevant since the tidal torque integral is proportional to the square of the coefficients. The (here prograde)  $n = 2$  harmonic is by far the strongest for low eccentricities. During orbital evolution, its excitation frequency  $\bar{\sigma}_2$  only crosses the resonance frequency of the weak prograde  $g_{20}^2$ -mode (i.e. the g-mode with  $l = 2$  which has 20 radial nodes). This happens at  $t \approx 7.2 \times 10^4$  yr, only 14 kyr after the (intrinsically weaker)  $n = 3$  harmonic crosses the much stronger  $g_{13}^2$  resonance peak. Around this time, the orbital period shows a small dip, mainly due to the  $n = 3$  resonance crossing. Because the  $g_{20}^2$  mode is the lowest frequency g-mode considered here, no further resonance crossings occur with the  $n = 2$  harmonic during the remaining orbital evolution. As the eccentricity drops during the orbital evolution, the  $n = 3$  Hansen coefficient is further decreased and the following  $n = 3$  resonance passages induce little or no features in the curve of the orbital period. Due to the off-resonant  $n = 2$  forcing frequency the star steadily spins up towards corotation.

For the  $n^{\text{th}}$  harmonic the time evolution of the eccentricity (12) can be expressed as

$$\frac{de^2}{dt} = 2 \frac{m-n}{H_{\text{orb}}} \mathcal{T}_n^{lm} + O(e^2). \quad (14)$$

Note that, initially, the star spins very sub-synchronously, so that the torque acting on the star  $m\mathcal{T}_n^{lm} > 0$  for all  $n$ . The  $n = 2$  harmonic of the  $m = 2$  potential does not give rise to significant changes in the eccentricity of the orbit because its circularizing effect vanishes to order  $O(e^2)$ . It appears that the potential term with  $n = 3$  is responsible for the strongest circularization effect, while the  $n = 1$  component could potentially increase the orbital eccentricity of the system. However, whereas the frequency  $\bar{\sigma}_1$  is so small that it does not cross any prograde resonance during the evolution of the orbit (although it does cross the r-modes around  $t = 0.8$  Myr), the  $n = 3$  forcing frequency starts between the g-modes with  $k = 12$  and  $k = 13$ , and passes through all of the modes  $g_{13}^2$  to  $g_{20}^2$  as the evolution progresses. Due to the small ratio  $(h_3^{3,2}/h_2^{3,2})^2 = (\frac{7}{2}e)^2$  the total torque on the star is dominated by the off-resonant  $n = 2$  contribution even when the  $n = 3$  forcing frequency is close to an eigen-frequency of the star. Therefore the rate  $\frac{d\bar{\sigma}_3}{dt}$  at which the  $n = 3$  frequency shifts through the spectrum varies only little. The g-modes with thirteen to twenty radial nodes roughly have  $\Delta\bar{\sigma} \approx 10^{-3}\bar{\sigma}_0$ . As only a few percent of the resonance peak area for such a peak is further than 10 peak widths away from the peak location, while the peaks are typically  $10^2$  peak widths apart, the tidal exchange rate due to the  $n = 3$  harmonic, and therefore the rate of change of the orbital eccentricity, is not equally distributed in time. Indeed, from Fig. 2c it is seen that only during a resonance passage the eccentricity of the system is significantly reduced, while only small eccentricity changes occur when  $\bar{\sigma}_3$  is in between resonances.

### 3.2. Example of resonance locking in a moderately eccentric ( $e = 0.25$ ) 5 day orbit

Let us now consider a moderately eccentric binary system with initially  $e = 0.25$  and orbital period  $P_{\text{orb}} = 5$  days, which has a periastron separation of  $D_{\text{per}}/R_s \approx 3.8$ . The initial rotation speed of the MS star is adopted to be 0.8 times the angular speed of the orbiting companion in periastron, or  $P_s \approx 3.6$  days. For this moderately eccentric orbit the harmonics of the tidal forcing run from  $n = 1$  to  $n_{\text{max}} = 17$  in our calculation. The maximum Hansen coefficient at  $t = 0$  corresponds to  $n = 2$ :  $h_2 = 0.85$ , while  $h_n < \frac{1}{2}h_2$  for  $n \geq 4$ . The orbital moment of inertia of the five day orbit is  $I_{\text{orb}} = 9.1 \times 10^{57} \text{ g cm}^2$ , while the stellar moment of inertia is  $I_s = 1.6 \times 10^{56} \text{ g cm}^2 \simeq I_{\text{orb}}/57$ . Since  $\frac{\partial\bar{\sigma}_{0,13}}{\partial\Omega_s} \simeq -0.15$  only, the factor  $\zeta = \left[ \frac{3n^2}{I_{\text{orb}}} - \frac{2}{I_s} \left( 2 + \frac{\partial\bar{\sigma}_{0,13}}{\partial\Omega_s} \right) \right]$  which appears in Eq. (10) becomes positive for  $n = 9$ , so that we expect locking to occur (if it occurs at all) with the harmonic  $n = 7$  or 8, which appears indeed to be the case. Because  $\bar{\sigma}_n$  and therefore  $\mathcal{T}_n^{lm}$  is negative for  $n \leq n_0 = 2$  and positive for  $n > 2$ , the locking conditions (11) apply when we consider locking of  $n = 7$ . Because of the relatively narrow and moderately eccentric orbit only a few low-order harmonics play a significant role in the orbital evolution of this system and the sums  $S_i$  in the locking conditions consist now of single terms. In Fig. 3 we plot the orbital evolution of this system. Three phases of rapid tidal dissipation can be discerned during which the orbital period and eccentricity decrease substantially. During the first phase of rapid evolution, around  $t = 0.2$  Myr, the initially sub-synchronously spinning star ( $\Omega_s = 0.8\omega_{\text{per}}$ ) is spun up to almost pseudo-corotation, while the orbital eccentricity decays from  $e = 0.25$  to  $\approx 0.19$ , in a few  $10^5$  years. This is a clear sign of resonance locking.

However, at  $t = 0$  no mode is resonantly excited, and the forcing frequency  $\bar{\sigma}_7$ , which is at the low frequency side of the prograde  $g_{13}^2$  mode, drifts towards the  $k = 13$  resonance peak mainly due to the combined effect of the star's evolution and driving by  $n = 2$ . This  $n = 2$  harmonic excites a non-resonant, heavily damped low frequency (short wavelength) response at a frequency in between retrograde  $g_{20}^2$  and the r-modes. The  $n = 2$  forcing thus induces a shift  $\Delta\bar{\sigma}_7$  which is insensitive to the exact value of  $\bar{\sigma}_2$  and, for a given magnitude of its Hansen coefficient, we can assume its effect to be approximately constant. Although the retrograde  $n = 2$  forcing term gives rise to the strongest *frequency shift*, its widening effect on the orbit is small compared to the orbital decay caused by the prograde forcing with  $n \geq 3$ , especially by the  $n = 7$  harmonic which approaches the resonance with  $g_{13}^2$ . This relatively strong mode is forced with high  $n$  and thus efficient in bringing down the orbital eccentricity and orbital period. In Fig. 4 we zoom in on the  $g_{13}^2$  resonance passage of the  $n = 7$  harmonic and plot the dominant contributions to the frequency shift of this harmonic.

At about  $t = 0.1$  Myr,  $\bar{\sigma}_7$  runs into the  $g_{13}^2$  resonance peak, and due to the negative sign of  $\zeta_{7,7}$  the associated tidal torque tends to shift the  $n = 7$  harmonic in the negative di-

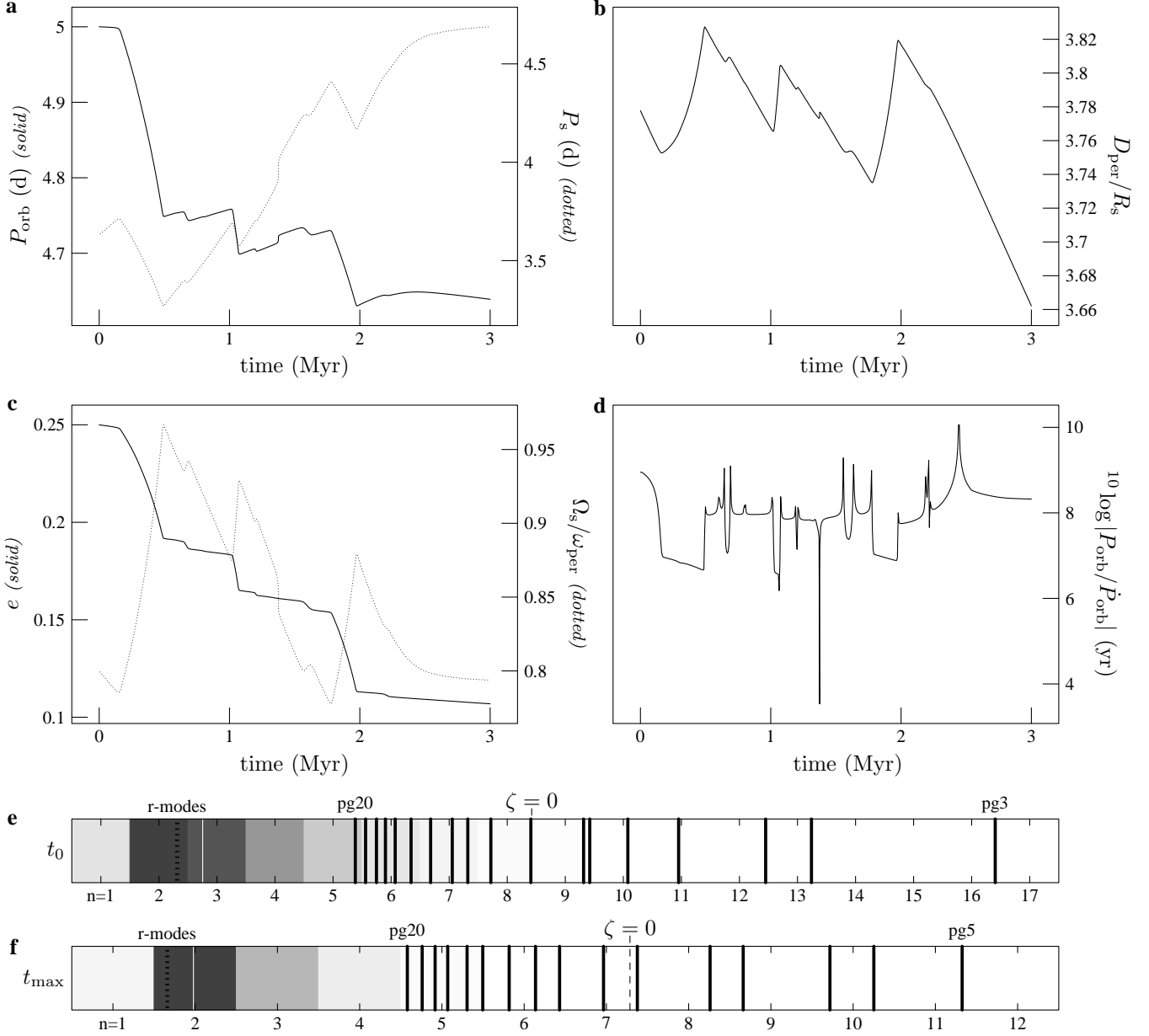


**Fig. 3.** Orbital evolution of a system with initial period  $P_{\text{orb}} = 5$  days and eccentricity  $e = 0.25$ . Initially the star rotates sub-synchronously ( $\Omega_s/\omega_{\text{per}} = 0.8$ ), but resonance locking of the  $n = 7$  harmonic of the tidal forcing quickly forces the star to spin near (pseudo) corotation. During the subsequent tidal evolution of the system, a few more cases of resonance locking (now with the  $n = 6$  harmonic) occur, recognisable by the more or less square shape of the dips in panel **d**, which shows the timescale for the orbital decay. **a** Orbital and stellar rotation period, **b** ratio of periastron distance to stellar radius, **c** eccentricity and ratio of stellar rotation frequency to orbital frequency at periastron, **d** timescale for the change of the size of the orbit, **e** and **f** schematic representation of the frequency distribution of forcing harmonics and stellar resonance frequencies at  $t = 0$  (panel **e**) and  $t = t_{\text{max}}$  (panel **f**).



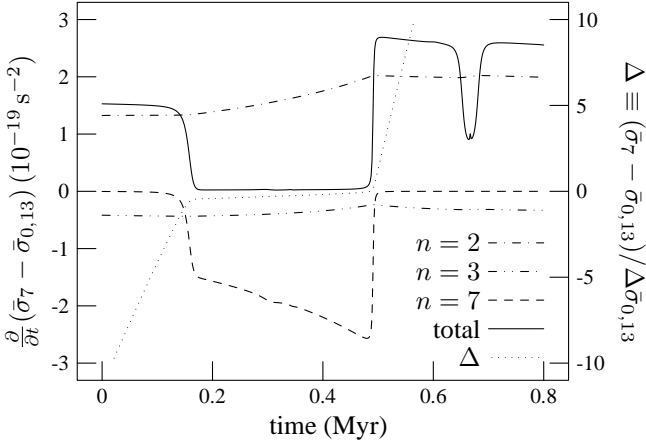


**Fig. 4.** Locking of the tidal harmonic  $n = 7$  onto the resonance with  $g_{13}^2$ . We plot the dominant contributions to the (rate of) frequency shifting of the  $n = 7$  harmonic relative to the resonance peak. The solid line gives the net rate of shifting by summing over all harmonics and adding the almost constant positive contribution of  $\simeq 10^{-19} \text{ s}^{-2}$  due to stellar evolution. The dotted line represents  $\Delta = (\bar{\sigma}_7 - \bar{\sigma}_{0,13})/\Delta\sigma$ , i.e. the distance to the peak of the resonance in units of the FWHM of the resonance peak.

rection, back out of the resonance. However, the thermonuclearly driven expansion of the MS star counteracts this tendency, while the retrograde  $n = 2$  harmonic pushes the  $n = 7$  harmonic even stronger into resonance. Although the  $g_{13}^2$  resonance gives an intrinsically much stronger response than the non-resonant  $n = 2$  response, the high order  $n = 7$  forcing is significantly weaker ( $(h_2/h_7)^2 \simeq 3.4 \times 10^2$ ) so that this effect is moderated. The  $n = 7$  harmonic thus gets trapped by the combined action of stellar evolution and the retrograde  $n = 2$  harmonic which drive the system into resonance against the resisting self-shift of the locked harmonic. Thereby the  $n = 7$  harmonic remains in close resonance with  $g_{13}^2$  during a few times  $10^5$  years, see dotted line in Fig. 4. Thanks to the relatively small value of  $|\zeta_{7,7}|$ , this locking occurs for a relatively large torque. Associated with the continuous resonant tidal interaction we see a rapid decline of the orbital eccentricity. This, however, weakens the tidal forcing of the  $n = 7$  harmonic and strengthens that of the  $n = 2$  harmonic. Thereby the  $n = 7$  harmonic is driven deeper and deeper into resonance with  $g_{13}^2$  until it can no longer withstand the growing positive frequency shift due to the  $n = 2$  component and passes the top of the resonance. Then the locking is broken and the  $n = 7$  harmonic suddenly moves through and away from the resonance. A similar, but shorter, locking phase occurs at  $t = 1.067$  Myr between  $n = 7$  and  $g_{12}^2$ . The dominant  $n = 2$  harmonic crosses the r-modes at  $t = 1.375$  Myr which can be observed in Fig. 3d as a single deep spike. Around  $t = 1.9$  Myr, the orbit now being narrower and  $\zeta = 0$  for  $n \simeq 7-8$ , a new prolonged locking phase sets in with  $n = 6$  and  $g_{14}^2$ . Fig. 3c shows that significant decay ( $\simeq 20\%$ ) of the orbital eccentricity occurs when a harmonic locks on to a (not particularly strong) resonance.

During these relatively short (of order  $\simeq 10^5$  years) locking phases the sub-synchronous star spins up considerably. However, the retrograde  $n = 2$  forcing, in combination with the continuous stellar expansion of the MS star brings the rotation rate down to small values. This continues until, near the end of the calculation, the stellar spin rate  $\Omega_s$  drops below the mean orbital speed  $\omega$  after which the  $m = n = 2$  harmonic becomes prograde. This brings the stellar spin down almost to a halt.

### 3.3. Tidal relaxation of a 10 day orbit with high ( $e = 0.7$ ) eccentricity.

Let us now illustrate the enhanced effectiveness of the tidal interaction in a highly eccentric orbit by showing that a system which has a 10 day orbit and  $e = 0.7$  will evolve towards tidal relaxation on a timescale short compared to the MS lifetime of the stellar component (which is approximately  $2 \times 10^7$  yr). Fig. 5 shows the evolution of such an orbit; at  $t = 0$  we adopt a stellar rotation rate equal to 0.7 times the orbital angular speed at periastron. As is seen from panel 5e, strong forcing occurs in the r-mode range of the stellar oscillation spectrum. Many prograde g-modes, including fairly strong ones, are in the wing of the Hansen distribution, creating many opportunities to transfer energy and angular momentum from the orbit to the star. Because of the location of  $\zeta = 0$ , far from any resonance, no locking is expected to occur during the initial stages of the orbital evolution.

Due to strong interaction with the stellar prograde g-modes the orbital period is halved during the first one million years. During this period the harmonics  $n = 9$  to 5 cross the r-modes, keeping the stellar rotation rate subsynchronous.

Between  $t = 1$  Myr and  $t = 3$  Myr the harmonic for which  $\zeta \simeq 0$  shifts further away from the r-modes, making the remaining r-mode crossings less effective, into the region of the stellar oscillation spectrum where strong g-modes are to be found. As a result, resonance locking with prograde g-modes occurs, spinning the star up to supersynchronous speed. During this period the dominant retrograde forcing of the  $n = 2$  harmonic, combined with the spin-down effect due to the stellar expansion, tends to slow down the stellar rotation. However, as long as resonance lockings of harmonics with higher  $n$ -values occur, the star is kept at a supersynchronous rotation speed. When around  $t = 3.1$  Myr the  $m = n = 2$  forcing frequency becomes prograde, the higher harmonics are no longer driven through the stellar oscillation spectrum in a direction opposite to their own shifting tendency, and equilibrium between two or more harmonics that produces resonance locking is no longer possible. At the end of the calculated evolution, when the system is significantly closer to the tidal equilibrium situation, the stellar spin-down due to stellar expansion and the spin-up due to the dominant low-frequency  $n = 2$  forcing reaches approximate equilibrium, whereby the shift of the forcing frequencies through the stellar oscillation spectrum progresses on the (long) nuclear timescale of the MS star. We expect full relaxation when the MS star approaches the end of core hydrogen

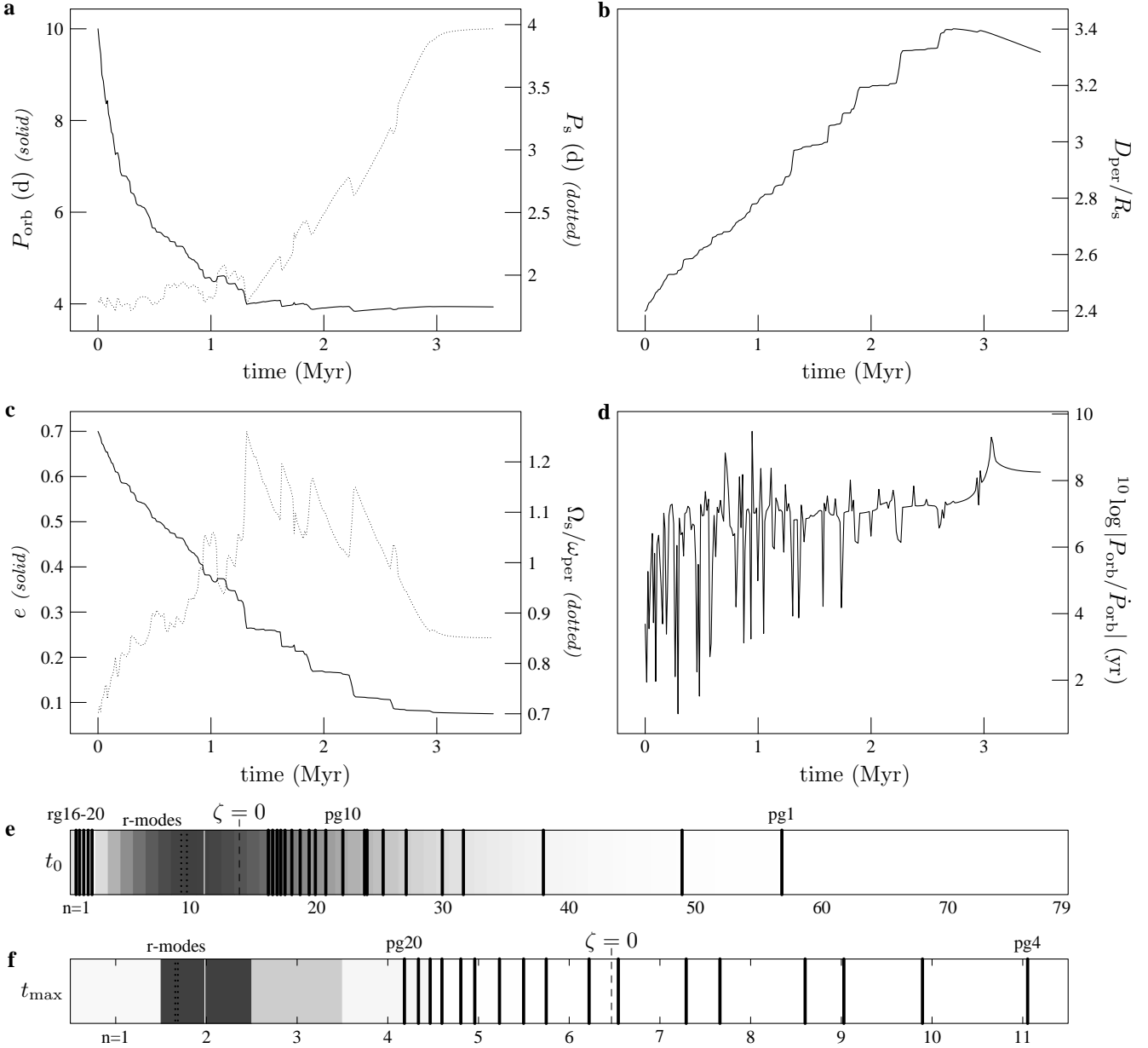


**Fig. 5.** Orbital relaxation in a fairly wide orbit with high eccentricity. At  $t = 0$  the orbital period is  $P_{\text{orb}} = 10$  days, the eccentricity is  $e = 0.7$ , and the star has central hydrogen abundance  $X_c = 0.40$ . The star is initially rotating at seventy percent of the orbital angular speed at periastron. Within 3 Myr the eccentricity is reduced to  $\simeq 0.08$ , and the orbit is shrunk to  $\simeq 4$  days. At  $t \simeq 3.1$  Myr the  $n = 2$  component in the forcing potential becomes prograde with respect to the stellar rotation. When its off-resonant spin-up effect comes into equilibrium with the spin-down effect of the stellar expansion, the orbital evolution progresses on a nuclear timescale. At this time, the stellar rotation speed relaxed to  $\simeq 0.85$  times quasi-synchronisation. **a** Orbital and stellar rotation period, **b** ratio of periastron distance to stellar radius, **c** eccentricity and ratio of stellar rotation frequency to orbital frequency at periastron, **d** timescale for the change of the size of the orbit, **e** and **f** schematic representation of the frequency distribution of forcing harmonics and stellar resonance frequencies at  $t = 0$  (panel **e**) and  $t = t_{\text{max}}$  (panel **f**).

burning and the stellar evolution speeds up considerably see (Savonije and Papaloizou, 1984).

#### 4. Results for wide binary systems: application to the binary pulsar PSR J0045-7319

Let us now consider systems similar to the SMC binary radio pulsar PSR J0045-7319, which has an orbital period of 51.17 days and an eccentricity of 0.8080. This binary system contains a B-star which, for an assumed  $1.4 M_{\odot}$  neutron star, has a mass  $(8.8 \pm 1.8) M_{\odot}$ . From the observed rather strong spin-orbit coupling the MS star is thought to be significantly deformed by rotation, i.e. it is thought to rotate rapidly with its spin axis inclined with respect to the orbital plane. The periastron distance for such a system is only  $\simeq 4$  stellar radii, and pulsar timing revealed that the orbit decays on a timescale of  $\frac{P_{\text{orb}}}{\dot{P}_{\text{orb}}} \simeq -5 \times 10^5$  yr (see Bell et al., 1995; Lai et al., 1995; Kaspi et al., 1996). Therefore, this system constitutes an ideal test laboratory for the study of stellar tides and neutron star birth kicks. According to Lai (1996; 1997), the short timescale of orbital decay suggests a significant retrograde stellar rotation with respect to the orbit. Indeed, Brandt & Podsiadlowski (1995) show from Monte Carlo simulations that after a supernova explosion, the spins of most stars in massive systems have large inclinations with respect to their orbital axes, and a significant fraction of systems ( $\sim 20$  percent) contain stars with retrograde spins. Kumar & Quataert (1997; 1998) argued that significant differential rotation, with a nearly synchronously rotating surface layer around a rapidly spinning interior, may be required to explain the observed timescale.

Although we cannot, at present, take into account the inclined orbit of PSR J0045-7319 we can study some aspects of this complex system. We will calculate the evolution of an aligned system with approximately the same orbital period and eccentricity, while adopting various values for the initial spin rate of the MS star: slightly super-synchronous rotation, highly super-synchronous rotation and retrograde rotation of the MS star. With ‘synchronous’ rotation we mean here of course a rotation rate equal to the orbital angular velocity of the companion at periastron. The initial eccentricity of  $e \simeq 0.8$  implies that the periastron frequency is  $\omega_{\text{per}} \simeq 15\omega$ . For such a highly eccentric orbit the tidal forcing is decomposed into a large number (of order  $10^2$ ) of harmonics, so that resonance crossings become ubiquitous (e.g. see Fig. 6d).

##### 4.1. Case a: slightly super-synchronous MS star

Let us start with a 51.17 day orbit, eccentricity  $e = 0.808$  and a stellar rotation rate  $\Omega_s = 1.1 \omega_{\text{per}}$ , i.e. the MS star is set to rotate 10% faster than the largest angular speed of the companion. This corresponds to an initial stellar rotation period  $P_s \simeq 3$  days. In Fig. 6e it can be seen that the retrograde g-modes ( $k \leq 20$ ) fall outside the tidal window. The dominant harmonics lie between  $9 < n < 43$ , all other harmonics have Hansen coefficients at least 50% weaker. The r-modes all cluster around harmonic  $n = 29$ , near the Hansen-peak and are thus

expected to be prominent in the following tidal evolution. The prograde g-modes ( $n_0 = 35$ ) from  $g_{20}$  to  $g_4$  can be excited, although they cover the range  $n > 62$  and thus lie in the weak wing of the Hansen curve, so that the resonances will be weak. The zero point of  $\zeta$  depends, for given  $m = 2$ , only weakly on  $k$  and corresponds to  $n = n_{\zeta} \simeq 40$ . Because there is no stellar mode which can be excited by this harmonic, we do not expect resonance locking to occur. Even when the stellar spin rate is decreased to zero the harmonics near  $\zeta = 0$  can excite only high radial order g-modes ( $k \simeq 18$ ) which seem too weak to induce efficient locking.

Let us now turn to the numerical results depicted in Fig. 6. As expected, very soon the  $n = 29$  harmonic of the  $l = m = 2$  tidal forcing comes into resonance with the fundamental r-mode  $r_0^3$ . After running through the whole range of r-modes (we consider  $k = 0$  to  $k = 10$  in our calculations, see Table B2 in Paper I) the same process repeats itself with the  $n = 28$  harmonic, etc. until finally, at  $t \simeq 4.3 \times 10^6$  yr, the  $n = 20$  harmonic runs through the r-mode range. Each time a harmonic runs through the r-mode range a new bump appears in the curve plotted in Figs. 6a and b because the r-modes transfer energy and angular momentum from the rapidly spinning star into the orbit in such a way that the semi-major axis and the eccentricity tend to increase. Eq. (12) shows that for the initial eccentricity  $e = 0.81$  the harmonics with  $5 < n < n_0 = 35$  will increase the orbital eccentricity, and the r-modes fall in this range. The effect of the evolutionary spin down of the star and of these repeated r-mode passages is that the star rapidly spins down to a sub-synchronous speed. The repetitive crossings of r-modes can also be seen in Fig. 6d. In between r-mode crossings the system now and then crosses a prograde g-mode ( $n \simeq 70$ –80 pass through  $g_{10}$  to  $g_{14}$ ) giving rise typically to orbital  $|P/\dot{P}| \simeq 10^6$  years. Due to the stellar spin down the prograde g-modes shift to lower frequencies so that stronger harmonics can excite them. This effect, in combination with relatively strong interaction with  $m = 0$  g-modes, becomes dominant after about  $t \simeq 2$  Myr whereby the orbital separation and eccentricity begin to decay (slowly). After 4 million years, the stellar rotation rate is reduced to approximately eighty percent of the pseudo-corotation rate ( $P_{\text{orb}} \simeq 4.2$  days) while the eccentricity, after an initial rise, is diminished by a small amount. We note that the effect of stellar expansion and despinning r-modes prevent the MS star from attaining approximate corotation in periastron, even while the periastron separation is quite small in this system.

##### 4.2. Case b: highly super-synchronous MS star

In this case we adopt the orbital parameters of case a, but the star is initially set to rotate at a higher rate:  $\Omega_s/\omega_{\text{per}} = 1.8$ . We still consider the case of stellar rotation in the same direction as the orbital motion of the companion. Fig. 7 gives the resulting orbital evolution, with the addition of a dotted line in panel 7d which gives the tidal timescale in case only forcing of the  $n = 48$  ( $m = 2$ ) harmonic would be taken into account. During some 1.1 Myr the tidal timescale, and therefore

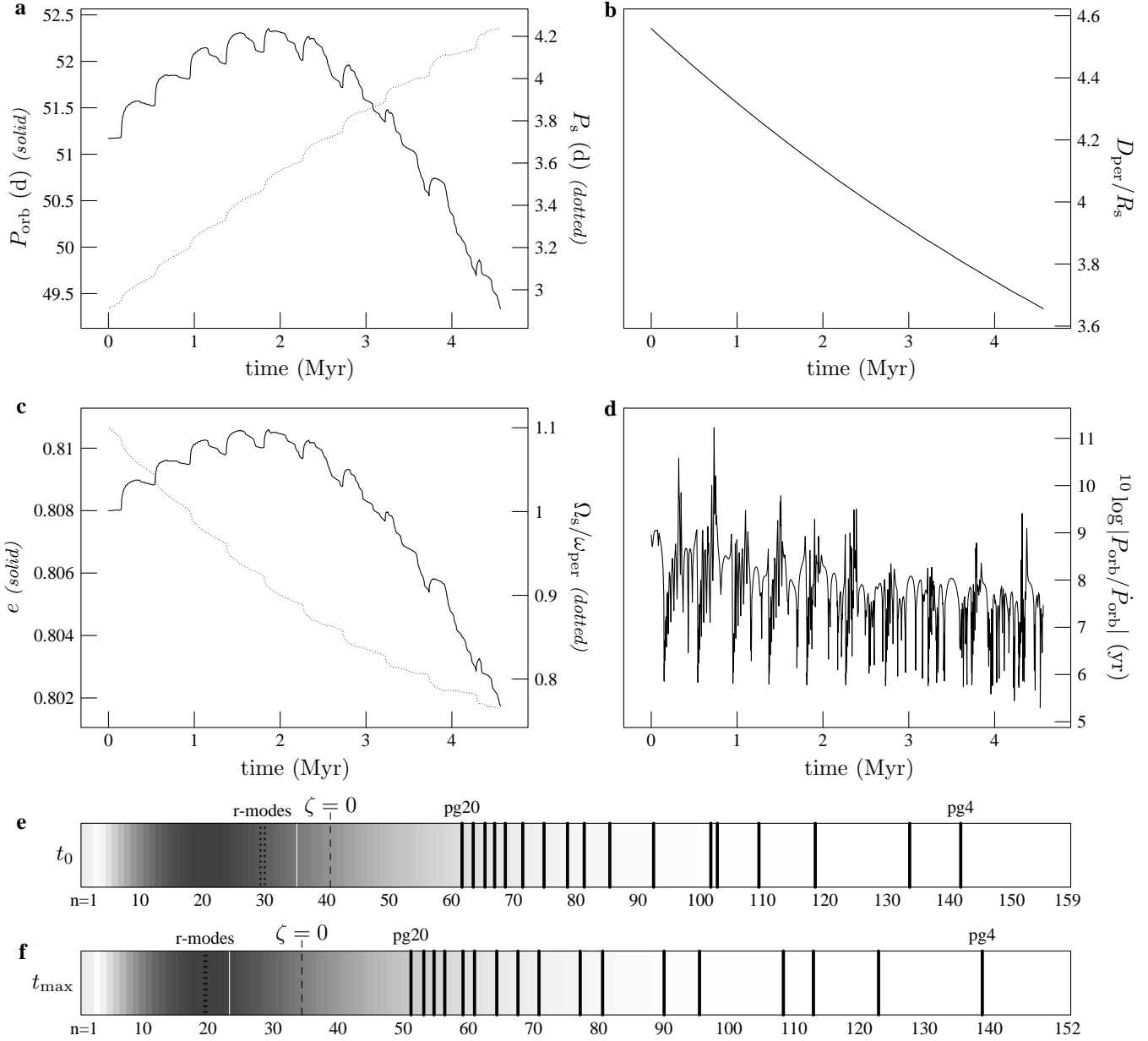


**Fig. 6.** Orbital evolution of a very eccentric ( $e = 0.808$ ) binary system with a 51.17 day orbital period. At  $t = 0$  the star rotates supersynchronously ( $\Omega_s/\omega_{\text{per}} = 1.1$ ), but by the continuous stellar expansion and resonant interaction with the (retrograde) r-modes the originally super-synchronous star is spun down to  $\simeq 0.8$  times periastron frequency (dotted line panel **c**). Each time that one of the tidal harmonics  $n = 29$  to  $n = 20$  runs through the r-modes the orbital period and eccentricity increase. This corresponds to the repetitive bumps in panels **a** and **b** and in deep repetitive spikes in panel **d**. After  $t \simeq 2$  Myr the prograde g-modes have shifted to lower frequencies (panel **e**) and become increasingly more prominent, so that the orbital separation and eccentricity slowly begin to decay. **a** Orbital and stellar rotation period, **b** ratio of periastron distance to stellar radius, **c** eccentricity and ratio of stellar rotation frequency to orbital frequency at periastron, **d** timescale for the change of the size of the orbit, **e** and **f** schematic representation of the frequency distribution of forcing harmonics and stellar resonance frequencies at  $t = 0$  (panel **e**) and  $t = t_{\text{max}}$  (panel **f**).

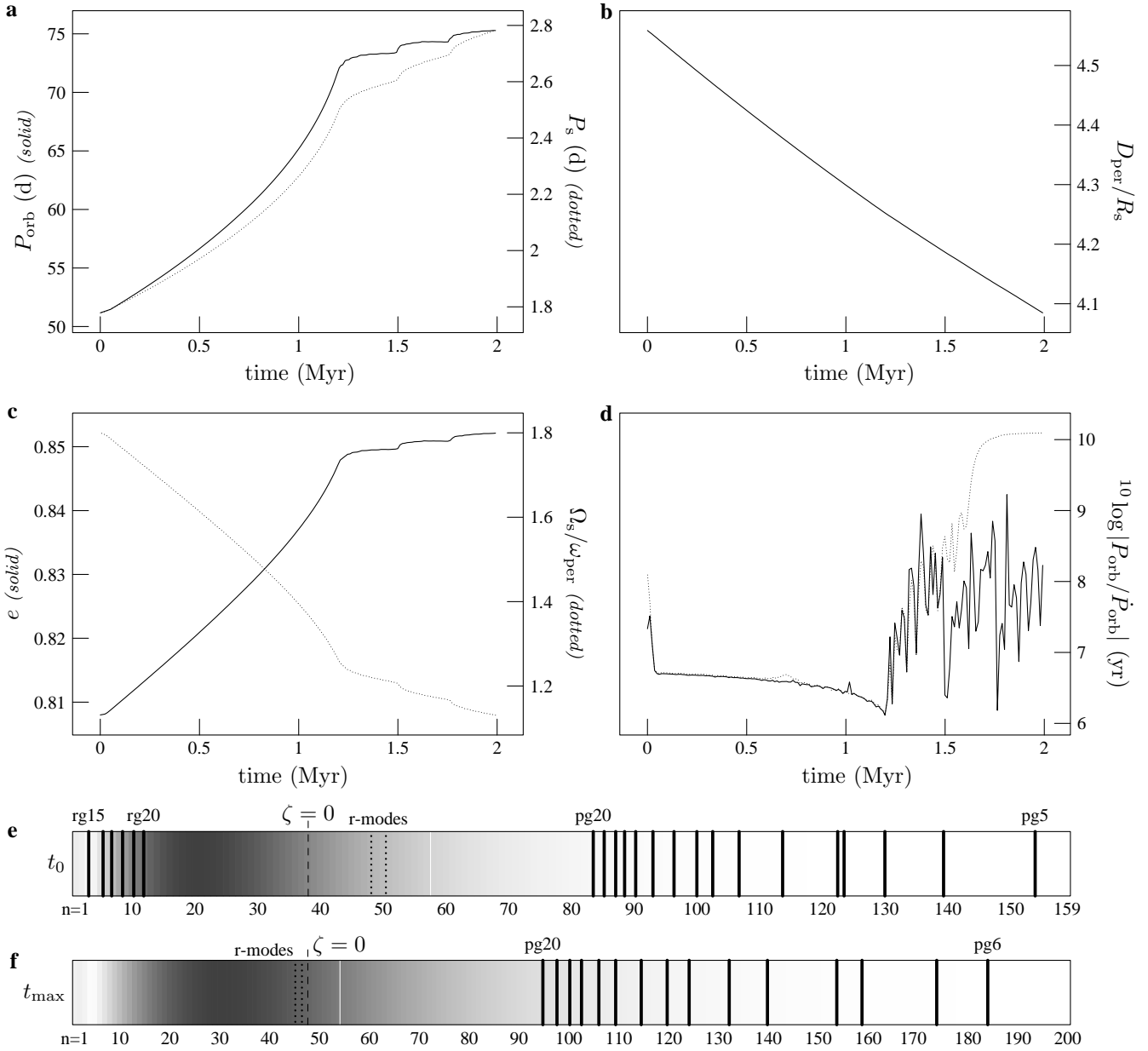


**Fig. 7.** Orbital evolution of a very eccentric binary system. At  $t = 0$  the system's parameters  $P_{\text{orb}} = 51.17$  days and  $e = 0.808$  are the same as for the orbit in Fig. 6, but the stellar rotation speed in this case is higher; 1.8 times the companion's angular speed at periastron. Very soon the  $n = 48$  harmonic in the potential runs into the fundamental r-mode and is locked near the resonance frequency for a period of more than one million years. During this period the star is spun down from 1.8 times periastron speed to less than 1.3 times periastron speed, while the orbital period is increased to approximately 72 days. During the locking the orbital eccentricity increases to almost 0.85. **a** Orbital and stellar rotation period, **b** ratio of periastron distance to stellar radius, **c** eccentricity and ratio of stellar rotation frequency to orbital frequency at periastron, **d** timescale for the change of the size of the orbit, **e** and **f** schematic representation of the frequency distribution of forcing harmonics and stellar resonance frequencies at  $t = 0$  (panel **e**) and  $t = t_{\text{max}}$  (panel **f**).

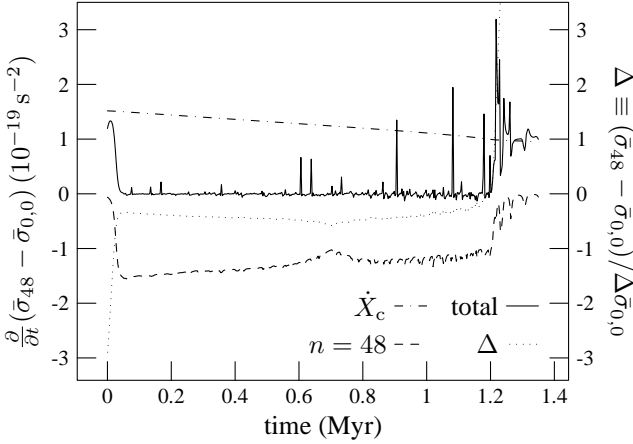


**Fig. 8.** Locking of the tidal harmonic  $n = 48$  onto the resonance with  $r_0^3$ . We plot the rate of frequency shifting of the  $n = 48$  harmonic relative to the resonance peak. The contribution due to stellar evolution is plotted dot-dashed, the contribution of the  $n = 48$  excitation itself is dashed. The solid line gives the net rate of shifting by summing over all harmonics and adding the contribution due to stellar evolution; the dotted line represents  $\Delta = (\bar{\sigma}_{48} - \bar{\sigma}_{0,0})/\Delta\sigma$ , i.e. the distance to the peak of the resonance in units of the FWHM of the resonance peak.

the acting torque, is dominated by the single contribution of this  $n = 48$  harmonic, indicating resonance locking.

Fig. 8 displays the rate of frequency shifting of the  $n = 48$  forcing frequency relative to the  $r_0^3$  resonance frequency. On average, the net rate of shifting is kept close to zero due to cancellation of the stellar evolution (positive) and  $n = 48$  (negative) contributions which are in equilibrium for some 1.1 Myr. The resonance passages of intrinsically strong (low radial order) prograde g-modes which occur (see Figs. 7e and 7f) induce only minor changes to the orbit and to the locking condition, due to their small corresponding Hansen coefficients, while passages of relatively strong harmonics through the retrograde g-mode resonances are unimportant because the modes which are crossed have many radial nodes and are thus intrinsically weak through strong damping. Although some of these resonance crossings do show up as spikes in the solid curve in Fig. 8, their duration is too short to significantly influence the resonance locking; many more of these spikes are not plotted due to graphical limitations. Only the passage of  $n = 49$  through  $r_6^3$  around  $t = 0.7$  Myr is able to briefly push the locked harmonic further from resonance. During evolution,  $\zeta_{48,48}$  is positive, but its value decreases as the orbit becomes wider. The ability of the locked mode to resist being pushed through resonance therefore weakens, and a larger torque is required to maintain the equilibrium, causing the harmonic forcing to drift closer towards the resonance peak. Eventually, the resonance is crossed and the locking is ended, which happens around  $t = 1.2$  Myr. After this happens the  $\bar{\sigma}_{48}$  forcing frequency drifts through the higher radial order r-modes, which have lower peak values and are unable to restore the locking

condition. The  $n = 47$  harmonic runs into the stellar  $r_0^3$  mode before the  $n = 48$  frequency reaches the last r-modes, and from this moment on the timescale (panel 7d) is no longer dominated by the action of the previously locked harmonic, but instead shows a sequence of dips below the dotted line which mark the r-mode resonance crossings of  $n = 47$ . Somewhat later ( $t \simeq 1.75$  Myr), the next harmonic with  $n = 46$  reaches the r-modes, causing a similar sequence of dips in the timescale curve.

#### 4.3. Case c: a retrograde spinning MS star

We will now consider the case where the star is spinning in the sense opposite to the orbital revolution of its compact companion, at thirty percent of its surface break-up speed. Furthermore we will adopt an initial orbital period  $P_{\text{orb}} = 55$  days, an eccentricity  $e = 0.81$  and a core hydrogen abundance  $X_c = 0.21$ , thus a fairly evolved MS star. For this initial configuration the tidal window is completely filled up with retrograde (in stellar frame) g-modes, see Fig. 9e. The peak of the Hansen distribution lies around harmonic  $n = 21$ , while the  $\zeta$ -factor vanishes for  $n \simeq 32$  which is near the resonance with  $g_{-10}^2$ . Thus under favourable circumstances this resonance may get locked, as will indeed be the case. Following the system until the core hydrogen content has been diminished to twenty percent, the orbital/spin evolution proceeds as depicted in Fig. 9.

At about  $t = 0.162$  Myr the  $n = 29$  harmonic approaches the resonance with  $g_{-10}^2$ , see Fig. 9a. The factor  $\zeta_{29,29}$ , or  $\zeta_{29}$  for short as defined in (10), being small from the very beginning, approaches zero and changes sign at  $t \simeq 0.167$  Myr. From this moment on, the self-shifting direction of the  $n = 29$  excitation is counter to the direction it has been shifting in, and it stops itself from passing the  $g_{-10}^2$  resonance frequency. Also, since  $\zeta_{29}$  is so close to zero, the torque associated with the resonant interaction hardly leads to a shift of the forcing frequency  $\bar{\sigma}_{29}$  and the locking can be very efficient. It depends on the action of the remaining harmonics whether the locking will last. The lower order harmonics with  $n < 29$  tend to push the  $n = 29$  forcing in the positive direction, i.e. deeper into resonance while the harmonics with  $n > 29$  tend to shift it back away from the resonance. Although the latter harmonics can excite strong low radial order g-modes, the peak of the Hansen distribution occurs for  $n \simeq 20$ , so that the low order harmonics dominate and keep the  $n = 29$  forcing close to resonance, see Fig. 10. The dotted curve in Fig. 9d and Fig. 10b represents the sole contribution of the  $n = 29$  harmonic to the decay time of the orbital period. It can be seen that from  $t \simeq 0.164$  Myr to  $t \simeq 0.171$  Myr most of the orbital decay is caused by the resonant interaction between  $n = 29$  and  $g_{-10}^2$ . During some 13 kyr the orbital decay time is between  $10^5$  and  $5 \times 10^5$  years, which is the observationally estimated decay time in PSR J0045-7319. Later in the evolution the  $n = 29$  harmonic causes more phases with a similar short decay time while exciting  $g_{-10}^2$ , but the  $\bar{\sigma}_{0,-10}$  resonance frequency is never crossed.

In our calculation with retrograde but aligned spin locking occurs for conditions slightly off the observed  $P_{\text{orb}}$  and

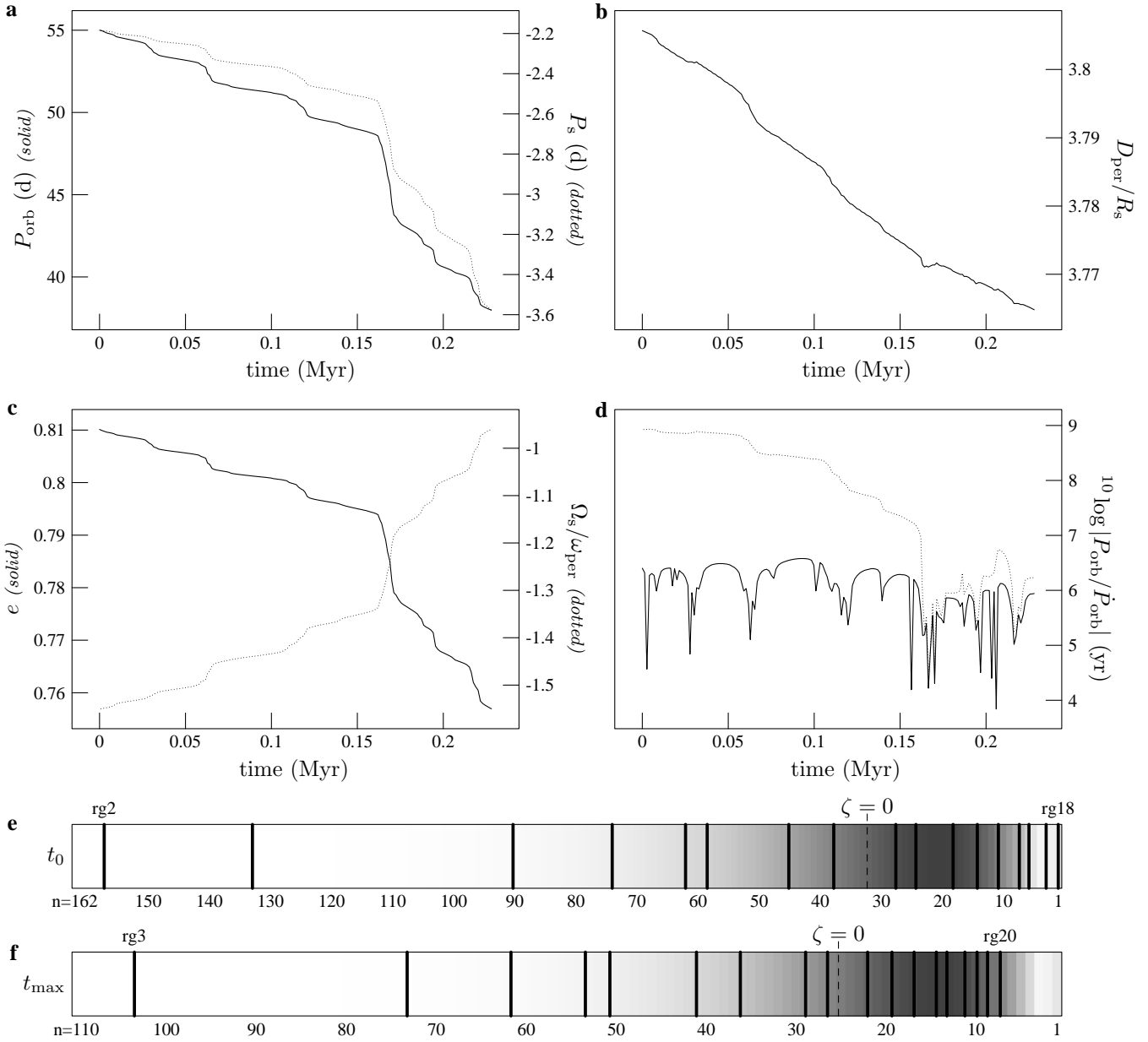


**Fig. 9.** Orbital evolution of a system mimicking PSR J0045-7319. At  $t = 0$  the orbital period is  $P_{\text{orb}} = 55$  days, the eccentricity is  $e = 0.81$ , and the star has central hydrogen abundance  $X_c = 0.21$  so that the periastron distance is initially approximately 3.8 stellar radii. The star initially has a retrograde rotation frequency of  $\Omega_s \simeq 0.3 \Omega_c$ . The large number of contributing tidal harmonics in the early stages of the orbital evolution frequently cause the timescale for orbital evolution (panel **d**) to reach values below  $10^5$  yr. A total of approximately 1000 resonance passages occur during the evolution shown, which is terminated as  $X_c$  reaches 0.2. **a** Orbital and stellar rotation period, **b** ratio of periastron distance to stellar radius, **c** eccentricity and ratio of stellar rotation frequency to orbital frequency at periastron, **d** timescale for the change of the size of the orbit, **e** and **f** schematic representation of the frequency distribution of forcing harmonics and stellar resonance frequencies at  $t = 0$  (panel **e**) and  $t = t_{\text{max}}$  (panel **f**).

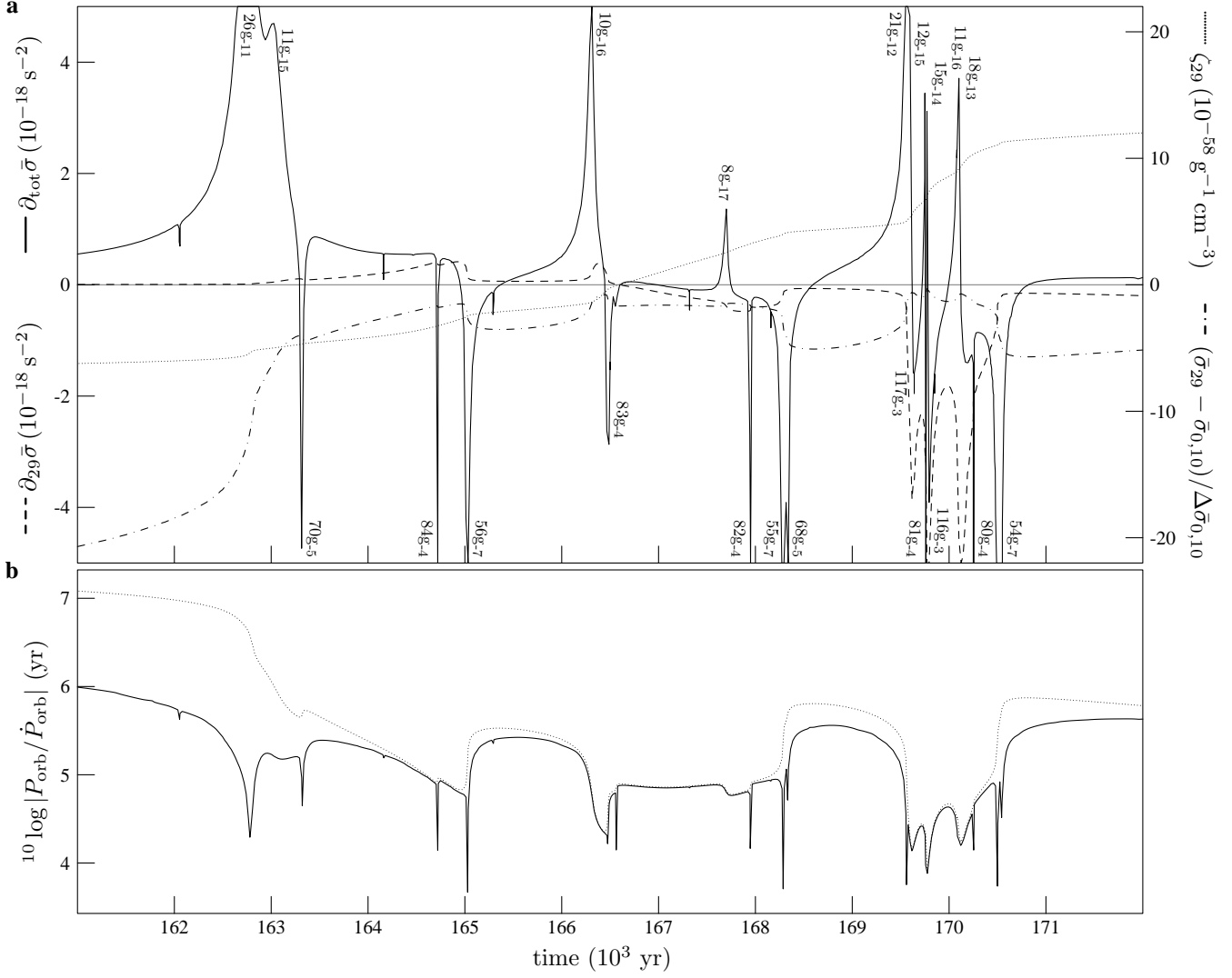


**Fig. 10.** Resonance locking of  $n = 29$  forcing harmonic on the retrograde  $g_{-10}^2$ -mode. **a** *Left ordinate:* net rate of relative  $(\bar{\sigma}_{29} - \bar{\sigma}_{0,10})$  frequency shifting due to the combined effect of all tidal harmonics and stellar evolution (solid line) and the shifting rate due to excitation of the  $n = 29$  term alone (dashed line). The nature of the resonance crossings is indicated along the solid line as  $ng_{-k}$ , where  $n$  gives the forcing harmonic and  $k$  the number of radial nodes of the excited oscillation. *Right ordinate:*  $\zeta_{29}$  (dotted line) and the distance between the  $n = 29$  forcing frequency and the  $k = 10$  retrograde g-mode resonance frequency. **b** Detail of panel 9d; characteristic timescale of orbital evolution (solid line) and characteristic timescale due to  $n = 29$  forcing alone (dotted line).



*e.* But note that the system parameters for which locking occurs depend on the details of the stellar input model and on the procedure for interpolating between the two evolution states  $X_c = 0.4$  and  $X_c = 0.2$ . We conclude that resonance locking might be responsible for the observed fast orbital decay in this system.

## 5. Discussion

We have studied the tidal evolution of eccentric early type binary systems by decomposing the time dependent tidal potential in a series of harmonics and by calculating the combined linear response of the uniformly rotating MS star with help of 2D-implicit code. We assumed the tidal oscillations to be in a steady state, whereby the tidal excitation is balanced by radiative damping. This allowed us to follow the orbital and spin evolution of the binary system in detail. However, during resonance crossings the assumptions of steady state and linearity may break down. Resonance peaks may sometimes be crossed on timescales short compared to their corresponding damping timescale  $\tau_d$ . As build-up of the full steady state response will take a number of damping times one may question the validity of the steady state approximation under these circumstances. In reality the resonance crossing will be slower, as the tidal response is not yet fully developed. However, the tidal evolution is not expected to be much different from our steady state results because the real evolution timescale is still likely to be significantly shorter than the timescales associated with the other (non-resonant) harmonics.

Non-linear effects can become significant during a resonance crossing with a weakly damped mode and may give rise either to enhanced or reduced tidal evolution, depending on circumstances. But note that non-linear effects may often be of less importance because strong tidal interaction generally implies rapid orbital and spin evolution away from the resonance, so that the oscillation amplitude is already limited by linear effects. Non-linear effects may influence resonance locking, whereby a harmonic remains near a resonance for a prolonged period of time. Non-linear damping might lower the resonance peak height and might thus diminish to some extent the duration of locking.

On the other hand, we have ignored the effect of resonances with  $l > 2$ . In a rotating star the dominant  $l = 2$  tidal component can excite (through the Coriolis force) also  $l = 4, 6, 8$  etc. modes, see Paper I. These higher spherical degree resonances will add additional resonance crossings during tidal evolution although for moderate stellar spin rates the peak area of these resonances is much less than that of the  $l = 2$  peaks. However, since peak area is not important for resonance locking, resonance locking may be even more important than our calculations show due to the denser oscillation spectrum.

## 6. Conclusion

Our calculations indicate that the many forcing harmonics present in orbits with significant eccentricity give rise to ef-

fective tidal evolution. By taking into account not only the orbital evolution, but also the evolution of the MS star – especially of its rotation rate – the system progresses through many resonances with stellar oscillation modes, a process that drives itself. Frequently conditions are favourable for resonance locking, whereby a particular tidal forcing harmonic is kept near-resonant with an oscillation mode for a prolonged period. Such phases lead to rapid orbital and spin evolution. It appears that fairly wide massive binary systems with large eccentricity can be almost circularized in a few million years. The observed short orbital decay time of the binary pulsar PSR J0045-7319 could be due to resonance locking if the stellar spin is retrograde.

*Acknowledgements.* This work was sponsored by the Stichting Nationale Computerfaciliteiten (National Computing Facilities Foundation, NCF) for the use of supercomputing facilities, with financial support from the Netherlands Organisation for Scientific Research (NWO) and by NWO Spinoza grant 08-0 to E.P.J. van den Heuvel.

## References

- Bell, J. F., Bessell, M. S., Stappers, B. W., Bailes, M., and Kaspi, V. M., 1995, *ApJ* 447, L117
- Brandt, N. and Podsiadlowski, P., 1995, *MNRAS* 274, 461
- Brouwer, D. and Clemence, G. M., 1961, *Methods of Celestial Mechanics*, Academic Press, New York
- Cowling, T. G., 1941, *MNRAS* 101, 367
- Eggleton, P. P., 1972, *MNRAS* 156, 361
- Iglesias, C. A. and Rogers, F. J., 1996, *ApJ* 464, 943
- Kaspi, V. M., Johnston, S., Bell, J. F., et al., 1994, *ApJ* 466, L43
- Kaspi, V. M., Bailes, M., Manchester, R. N., Stappers, B. W., and Bell, J. F., 1996, *Nat* 381, 584
- Kumar, P. and Goodman, J., 1996, *ApJ* 466, 946
- Kumar, P. and Quataert, E. J., 1997, *ApJ* 479, L51
- Kumar, P. and Quataert, E. J., 1998, *ApJ* 493, 412
- Lai, D., 1996, *ApJ* 466, L35
- Lai, D., 1997, *ApJ* 490, 847
- Lai, D., Bildsten, L., and Kaspi, V. M., 1995, *ApJ* 452, 819
- Landau, L. D. and Lifshitz, E. M., 1959, *Mechanics*, Pergamon Press, New York
- Morse, P. M. and Feshbach, H., 1952, *Methods of Theoretical Physics*, Vol. II, McGraw Hill Book Comp., Tokyo
- Papaloizou, J. C. B. and Pringle, J. E., 1978, *MNRAS* 182, 423
- Pols, O. R., Tout, C. A., Eggleton, P. P., and Han, Z., 1995, *MNRAS* 274, 964
- Savonije, G. J. and Papaloizou, J. C. B., 1983, *MNRAS* 203, 581
- Savonije, G. J. and Papaloizou, J. C. B., 1984, *MNRAS* 207, 685
- Savonije, G. J. and Papaloizou, J. C. B., 1997, *MNRAS* 291, 633
- van den Heuvel, E. P. J. and Heise, J., 1972, *Nature Phys. Sc.* 239, 67
- Witte, M. G. and Savonije, G. J., 1999, *A&A* 341, 842, Paper I
- Zahn, J. P., 1977, *A&A* 57, 383

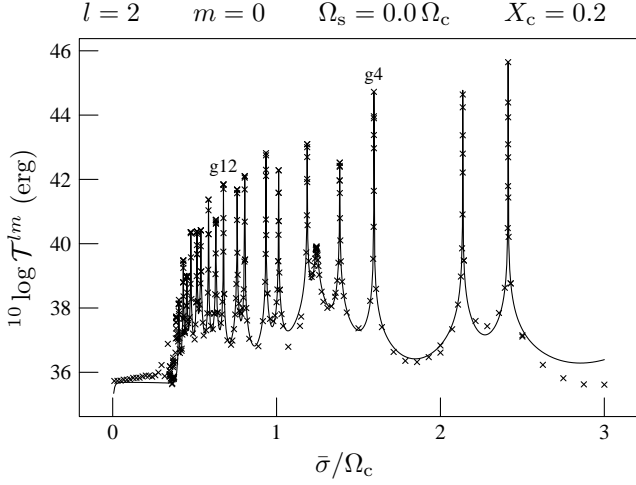


**Fig. A1.** Torque integral  $\mathcal{T}^{lm}$  versus forcing frequency  $\bar{\sigma}$  for forcing with  $l = 2$  and  $m = 0$  on a  $10 M_\odot$  non-rotating star. Prograde  $g_k^2$ -modes with  $k = 4$  and  $11$  are labelled. Crosses denote calculated points, while the solid curve represents a fit.

## Appendix A: Determination of the tidal torque

In Paper I we calculated the non-adiabatic tidal response of a uniformly rotating, somewhat evolved ( $X_c = 0.4$ ),  $10 M_\odot$  main sequence star to the dominant  $l = 2$  components of its compact  $1 M_\odot$  binary companion's tidal potential for a wide range of prograde and retrograde forcing frequencies and determined the corresponding tidal torques on the MS star. The relative orbit of the compact star was assumed circular and with a fixed separation of 4 stellar radii (of the MS star). In order to include effects of stellar evolution on the tidal evolution of the orbit, we have now calculated additional torque spectra for a stellar model with core hydrogen abundance (mass fraction)  $X_c = 0.2$ , the results of which are listed in Tables B1 and B2.

Both stellar models, comprising 1200 (radial) zones, were calculated using the stellar evolution code developed by Eggleton (1972) and more recently revised by Pols et al. (1995), with the addition of recent OPAL opacity Tables (Iglesias and Rogers, 1996).

The model with  $X_c = 0.4$  has a stellar radius equal to  $R_s = 3.825 \times 10^{11}$  cm, an effective temperature  $T_{\text{eff}} = 2.314 \times 10^4$  K and a stellar moment of inertia  $I_s = 1.55 \times 10^{56}$  g cm<sup>2</sup>. The break-up angular speed equals  $\Omega_c = 1.54 \times 10^{-4}$  s<sup>-1</sup>. The model with  $X_c = 0.2$ , on the other hand, has a radius  $R_s = 4.807 \times 10^{11}$  cm, an effective temperature  $T_{\text{eff}} = 2.157 \times 10^4$  K, moment of inertia  $I_s = 2.059 \times 10^{56}$  g cm<sup>2</sup> and break-up angular frequency  $\Omega_c = 1.095 \times 10^{-4}$  s<sup>-1</sup>.

Fig. A1 shows the calculated torque integral spectrum for  $m = 0$  forcing on the non-rotating star; compared to the  $X_c = 0.4$  data, the degree of central condensation in the star has increased, the resonance frequencies of the stellar g-modes shift to much higher dimensionless values  $\bar{\sigma}_0/\Omega_c$ . The break-up frequency  $\Omega_c$  however, drops due to the increasing stellar radius, such that the actual frequency of the modes on average increases by only a few ( $\simeq 5$ ) percent. It is also seen that the

spacing between the individual modes is very different for the two stellar models. Different modes react differently upon the changes in the stellar structure, resulting in seemingly random shifting of the peaks superimposed on the global trend towards higher dimensionless frequencies.

For  $X_c = 0.2$  we synthesise g-mode spectra for  $\Omega_s = 0.2, 0.3$  and  $0.4 \Omega_c$  by normalising the peak widths and areas from the  $m = 0, \Omega_s = 0.0 \Omega_c, X_c = 0.4$  spectrum from Paper I to the  $m = 0, \Omega_s = 0.0 \Omega_c$  spectrum for  $X_c = 0.2$  and assuming that the deducted ratios apply to the other stellar rotation rates as well. We also assume that the coefficients  $c_j$  for the  $\Omega_s$ -dependence  $\frac{\bar{\sigma}_0}{\Omega_c} = \sum c_j \left(\frac{\Omega_s}{\Omega_c}\right)^j$  of the resonance frequencies calculated for the  $X_c = 0.4$  model in Paper I can be used for the  $X_c = 0.2$  spectra.

At low forcing frequencies where the resonant g-mode oscillations attain high radial orders the values of  $\mathcal{T}^{lm}$  are dominated by the turbulent dissipation in convective regions (see Paper I). For the orbital evolution calculations of this paper we approximate the torque integral in these frequency regions by a small constant level. For the non rotating  $X_c = 0.4$  model this level is  $1 \times 10^{37}$  erg, for the  $X_c = 0.2$  model it is  $5 \times 10^{35}$  erg. In a rotating model the calculated torque values in the retrograde frequency domain around the r-modes become larger. Here we multiply the level with a factor  $(1 + 10\Omega_s/\Omega_c)$  to approximately fit this effect. The area  $\Delta\bar{\sigma}\mathcal{T}^{lm}$  of this low frequency interval of the stellar spectrum is not very large, and compares to the peak area of a g-mode with approximately 15 radial nodes; much less than the peak area of the low radial order g-modes (1 to 10 radial nodes). Under many circumstances, this regime will therefore not play an important role in the evolution of the orbit. Under some circumstances however, e.g. if many strong tidal harmonics have frequencies in the designated area, or if only few harmonics are present in the forcing potential and the strongest one has its frequency in this domain (as is the case during resonance locking in moderately eccentric orbits, see Sect. 3.2), the details of our orbital calculations are subject to uncertainties due to the numerical limitation of having to work with a finite mesh and due to the theoretical limitation of not having a sound theory for turbulent convection. Nevertheless, the calculations presented here are believed to give a qualitative picture of the process of tidal evolution and are useful as an order of magnitude estimate for the strength of the occurring effects.

### A.1. Interpolation procedure for the tidal torque

For each forcing frequency  $\bar{\sigma}_n$ , the corresponding torque integral  $\mathcal{T}_n^{lm}$  is calculated by interpolation in the Tables of Appendix B: and those in the appendix of Paper I in terms of the three state parameters: forcing frequency  $\bar{\sigma}_n$ , stellar rotation rate  $\Omega_s$  and evolutionary state of the star  $X_c$  (i.e. the hydrogen content of the convective core). Subsequently the obtained torque values are normalised by a factor  $(M_p/M_\odot)^2 (4R_s/a)^{(2l+2)} (h_n^{(l+1),m})^2$  as the torque integrals

have been calculated for a  $1 M_{\odot}$  companion in a fixed circular orbit with  $a = 4R_s$ .

To perform interpolations in  $\Omega_s$ , linear relations were used for  $\Delta\bar{\sigma}$  and the peak area  $\pi\Delta\bar{\sigma}\mathcal{T}_0^{lm}$ , while polynomial interpolations of the highest possible order were used for the resonance frequencies  $\bar{\sigma}_0$ . For  $\bar{\sigma}_0$ , we assumed the derivative  $\frac{d\bar{\sigma}_0}{d\Omega_s}$  for  $m = 0$  modes to vanish for a non-rotating star (from symmetry), and for r-modes to become  $-\frac{1}{3}$  in order to obey the asymptotic value  $\bar{\sigma} = -\frac{2m}{l(l+1)}\Omega_s$  with  $l = 3$  and  $m = 2$ . The r-mode resonance frequencies were fitted by  $\frac{\bar{\sigma}_0}{\Omega_s} = -\frac{1}{3}x + c_2x^2 + c_3x^3 + c_4x^4 + c_5x^5$  with  $x = \Omega_s/\Omega_c$ , whereby the polynomial coefficients are listed in Table B3.

Linear interpolations are used between the  $X_c = 0.4$  and  $X_c = 0.2$  models for the peak widths and areas and the frequency  $\bar{\sigma}_0$  and polynomial coefficients  $c_j$  of each mode  $n$  in the spectra, and for the stellar radius and moment of inertia.

As the calculated resonance peaks are accurately represented by the harmonic oscillator fits, the peak width of the fits can be assumed to give a good measure of the damping timescale  $\tau_d = \frac{2\pi}{\Delta\bar{\sigma}}$  of the excited modes. From the tabulated peak widths we find that for all calculated g-modes  $\tau_d$  lies between  $\sim 45$  days and  $\sim 10^3$  yr; for the r-modes  $\tau_d$  varies between  $\sim 200$  days and  $\sim 200$  years unless the stellar rotation drops below  $0.1 \Omega_c$ , in which case both the strength of the modes and the damping rate is strongly reduced.

While evolving the orbit, timesteps are chosen in such a manner that no frequency component  $\bar{\sigma}_n$  will travel more than what corresponds to five percent of the height of a resonance peak per timestep.

## Appendix B: Tables

**Table B1.** Fitting parameters for  $g_k^2$ -mode resonances with an  $l = 2, m = 0$  tidal potential in a  $10 M_\odot$  star with  $X_c = 0.2$ . All tabulated values for the torque integral have been obtained for a fixed orbital separation.

$\Omega_s = 0.0 \Omega_c$											
$k$	$\bar{\sigma}_0/\Omega_c$	$\mathcal{T}_0^{lm}$ (erg)	$\Delta\bar{\sigma}/\Omega_c$	$k$	$\bar{\sigma}_0/\Omega_c$	$\mathcal{T}_0^{lm}$ (erg)	$\Delta\bar{\sigma}/\Omega_c$	$k$	$\bar{\sigma}_0/\Omega_c$	$\mathcal{T}_0^{lm}$ (erg)	$\Delta\bar{\sigma}/\Omega_c$
1	3.4254	$1.23 \times 10^{46}$	$1.14 \times 10^{-5}$	8	1.0127	$1.94 \times 10^{42}$	$2.06 \times 10^{-4}$	15	0.5382	$2.63 \times 10^{40}$	$8.91 \times 10^{-4}$
2	2.4130	$4.53 \times 10^{45}$	$1.16 \times 10^{-5}$	9	0.9356	$7.18 \times 10^{42}$	$1.00 \times 10^{-4}$	16	0.5142	$2.45 \times 10^{40}$	$7.41 \times 10^{-4}$
3	2.1362	$5.93 \times 10^{44}$	$2.93 \times 10^{-5}$	10	0.8057	$1.28 \times 10^{42}$	$1.81 \times 10^{-4}$	17	0.4768	$2.30 \times 10^{40}$	$5.76 \times 10^{-4}$
4	1.5940	$5.29 \times 10^{44}$	$2.34 \times 10^{-5}$	11	0.7592	$4.86 \times 10^{41}$	$2.97 \times 10^{-4}$	18	0.4528	$1.21 \times 10^{39}$	$1.91 \times 10^{-3}$
5	1.3853	$3.32 \times 10^{42}$	$4.26 \times 10^{-4}$	12	0.6759	$7.13 \times 10^{41}$	$1.64 \times 10^{-4}$	19	0.4309	$3.13 \times 10^{39}$	$8.79 \times 10^{-4}$
6	1.2434	$7.90 \times 10^{39}$	$1.48 \times 10^{-2}$	13	0.6298	$5.57 \times 10^{40}$	$6.70 \times 10^{-4}$	20	0.4039	$1.72 \times 10^{38}$	$1.69 \times 10^{-3}$
7	1.1867	$1.26 \times 10^{43}$	$2.49 \times 10^{-4}$	14	0.5846	$2.35 \times 10^{41}$	$2.43 \times 10^{-4}$				

**Table B2.** Fitting parameters for  $r_k^3$ -mode resonances with an  $l = 2, m = 2$  tidal potential in a  $10 M_\odot$  star with  $X_c = 0.2$ . All tabulated values for the torque integral have been obtained for a fixed orbital separation.

$\Omega_s = 0.1 \Omega_c$						$\Omega_s = 0.2 \Omega_c$		
$k$	$\bar{\sigma}_0/\Omega_c$	$\mathcal{T}_0^{lm}$ (erg)	$\Delta\bar{\sigma}/\Omega_c$	$k$	$\bar{\sigma}_0/\Omega_c$	$\mathcal{T}_0^{lm}$ (erg)	$\Delta\bar{\sigma}/\Omega_c$	
0	$-3.3263 \times 10^{-2}$	$-5.52 \times 10^{40}$	$8.80 \times 10^{-6}$	0	$-6.6207 \times 10^{-2}$	$-7.84 \times 10^{40}$	$1.15 \times 10^{-4}$	
1	$-3.3245 \times 10^{-2}$	$-1.16 \times 10^{41}$	$1.33 \times 10^{-5}$	1	$-6.6068 \times 10^{-2}$	$-6.62 \times 10^{40}$	$1.70 \times 10^{-4}$	
2	$-3.3183 \times 10^{-2}$	$-9.61 \times 10^{40}$	$2.13 \times 10^{-5}$	2	$-6.5662 \times 10^{-2}$	$-1.19 \times 10^{41}$	$1.28 \times 10^{-4}$	
3	$-3.3111 \times 10^{-2}$	$-1.11 \times 10^{41}$	$1.41 \times 10^{-5}$	3	$-6.5083 \times 10^{-2}$	$-9.97 \times 10^{40}$	$1.24 \times 10^{-4}$	
4	$-3.3016 \times 10^{-2}$	$-5.06 \times 10^{40}$	$2.32 \times 10^{-5}$	4	$-6.4357 \times 10^{-2}$	$-5.07 \times 10^{40}$	$1.71 \times 10^{-4}$	
5	$-3.2896 \times 10^{-2}$	$-2.83 \times 10^{40}$	$2.86 \times 10^{-5}$	5	$-6.3476 \times 10^{-2}$	$-2.88 \times 10^{40}$	$1.96 \times 10^{-4}$	
6	$-3.2756 \times 10^{-2}$	$-1.53 \times 10^{40}$	$3.48 \times 10^{-5}$	6	$-6.2463 \times 10^{-2}$	$-1.51 \times 10^{40}$	$2.52 \times 10^{-4}$	
7	$-3.2597 \times 10^{-2}$	$-9.62 \times 10^{39}$	$4.16 \times 10^{-5}$	7	$-6.1355 \times 10^{-2}$	$-9.73 \times 10^{39}$	$2.86 \times 10^{-4}$	
8	$-3.2427 \times 10^{-2}$	$-5.51 \times 10^{39}$	$5.33 \times 10^{-5}$	8	$-6.0210 \times 10^{-2}$	$-5.95 \times 10^{39}$	$3.30 \times 10^{-4}$	
9	$-3.2249 \times 10^{-2}$	$-2.77 \times 10^{39}$	$5.89 \times 10^{-5}$	9	$-5.9058 \times 10^{-2}$	$-3.05 \times 10^{39}$	$3.67 \times 10^{-4}$	
10	$-3.2061 \times 10^{-2}$	$-7.40 \times 10^{38}$	$7.54 \times 10^{-5}$	10	$-5.7878 \times 10^{-2}$	$-8.50 \times 10^{38}$	$4.14 \times 10^{-4}$	
$\Omega_s = 0.3 \Omega_c$						$\Omega_s = 0.4 \Omega_c$		
$k$	$\bar{\sigma}_0/\Omega_c$	$\mathcal{T}_0^{lm}$ (erg)	$\Delta\bar{\sigma}/\Omega_c$	$k$	$\bar{\sigma}_0/\Omega_c$	$\mathcal{T}_0^{lm}$ (erg)	$\Delta\bar{\sigma}/\Omega_c$	
0	$-9.8673 \times 10^{-2}$	$-7.42 \times 10^{40}$	$2.23 \times 10^{-4}$	0	$-1.3043 \times 10^{-1}$	$-7.38 \times 10^{40}$	$3.69 \times 10^{-4}$	
1	$-9.8199 \times 10^{-2}$	$-9.27 \times 10^{40}$	$3.88 \times 10^{-4}$	1	$-1.2937 \times 10^{-1}$	$-1.08 \times 10^{41}$	$7.91 \times 10^{-4}$	
2	$-9.6772 \times 10^{-2}$	$-1.18 \times 10^{41}$	$4.08 \times 10^{-4}$	2	$-1.2598 \times 10^{-1}$	$-1.33 \times 10^{41}$	$7.57 \times 10^{-4}$	
3	$-9.4960 \times 10^{-2}$	$-9.47 \times 10^{40}$	$4.17 \times 10^{-4}$	3	$-1.2199 \times 10^{-1}$	$-8.80 \times 10^{40}$	$9.93 \times 10^{-4}$	
4	$-9.2676 \times 10^{-2}$	$-5.45 \times 10^{40}$	$4.50 \times 10^{-4}$	4	$-1.1721 \times 10^{-1}$	$-5.28 \times 10^{40}$	$9.91 \times 10^{-4}$	
5	$-9.0077 \times 10^{-2}$	$-2.73 \times 10^{40}$	$6.36 \times 10^{-4}$	5	$-1.1189 \times 10^{-1}$	$-2.81 \times 10^{40}$	$1.14 \times 10^{-3}$	
6	$-8.7159 \times 10^{-2}$	$-1.53 \times 10^{40}$	$6.86 \times 10^{-4}$	6	$-1.0630 \times 10^{-1}$	$-1.39 \times 10^{40}$	$1.47 \times 10^{-3}$	
7	$-8.4114 \times 10^{-2}$	$-9.92 \times 10^{39}$	$7.52 \times 10^{-4}$	7	$-1.0076 \times 10^{-1}$	$-1.01 \times 10^{40}$	$1.36 \times 10^{-3}$	
8	$-8.1102 \times 10^{-2}$	$-6.13 \times 10^{39}$	$8.90 \times 10^{-4}$	8	$-9.5551 \times 10^{-2}$	$-6.59 \times 10^{39}$	$1.42 \times 10^{-3}$	
9	$-7.8246 \times 10^{-2}$	$-3.40 \times 10^{39}$	$8.35 \times 10^{-4}$	9	$-9.0814 \times 10^{-2}$	$-3.84 \times 10^{39}$	$1.44 \times 10^{-3}$	
10	$-7.5465 \times 10^{-2}$	$-1.01 \times 10^{39}$	$9.48 \times 10^{-4}$	10	$-8.6386 \times 10^{-2}$	$-1.17 \times 10^{39}$	$1.69 \times 10^{-3}$	

**Table B3.** Coefficients  $c_j$  for the  $\Omega_s$ -dependence  $\bar{\sigma}_0 = \sum c_j \left(\frac{\Omega_a}{\Omega_c}\right)^j$  of the resonance frequency of r-modes in a  $10 M_\odot$  star with  $X_c = 0.4$  and  $X_c = 0.2$ . ( $c_1 = -\frac{1}{3}$ )

$X_c = 0.4$				
$k$	$c_2$	$c_3$	$c_4$	$c_5$
0	$9.76 \times 10^{-3}$	$-3.29 \times 10^{-2}$	$3.61 \times 10^{-1}$	$-4.23 \times 10^{-1}$
1	$1.39 \times 10^{-2}$	$-3.55 \times 10^{-2}$	$4.32 \times 10^{-1}$	$-4.42 \times 10^{-1}$
2	$9.65 \times 10^{-3}$	$7.34 \times 10^{-2}$	$3.53 \times 10^{-1}$	$-5.10 \times 10^{-1}$
3	$3.69 \times 10^{-3}$	$2.73 \times 10^{-1}$	$-5.79 \times 10^{-2}$	$-1.51 \times 10^{-1}$
4	$2.25 \times 10^{-4}$	$4.77 \times 10^{-1}$	$-4.43 \times 10^{-1}$	$2.60 \times 10^{-1}$
5	$1.90 \times 10^{-3}$	$6.25 \times 10^{-1}$	$-3.86 \times 10^{-1}$	$-2.19 \times 10^{-1}$
6	$-1.38 \times 10^{-3}$	$8.98 \times 10^{-1}$	$-8.40 \times 10^{-1}$	$-1.22 \times 10^{-1}$
7	$-5.59 \times 10^{-3}$	1.23	-1.59	$3.45 \times 10^{-1}$
8	$-1.27 \times 10^{-2}$	1.64	-2.73	1.33
9	$-1.60 \times 10^{-2}$	2.00	-3.68	1.99
10	$-3.45 \times 10^{-2}$	2.68	-6.37	5.16
$X_c = 0.2$				
$k$	$c_2$	$c_3$	$c_4$	$c_5$
0	$-2.46 \times 10^{-5}$	$8.78 \times 10^{-2}$	$-1.96 \times 10^{-1}$	$2.26 \times 10^{-1}$
1	$7.17 \times 10^{-4}$	$9.32 \times 10^{-2}$	$-1.37 \times 10^{-1}$	$1.37 \times 10^{-1}$
2	$7.10 \times 10^{-3}$	$6.44 \times 10^{-2}$	$1.75 \times 10^{-1}$	$-2.33 \times 10^{-1}$
3	$4.54 \times 10^{-3}$	$1.77 \times 10^{-1}$	$1.06 \times 10^{-2}$	$-9.57 \times 10^{-2}$
4	$5.30 \times 10^{-3}$	$2.61 \times 10^{-1}$	$6.76 \times 10^{-2}$	$-3.09 \times 10^{-1}$
5	$3.38 \times 10^{-3}$	$4.22 \times 10^{-1}$	$-1.60 \times 10^{-1}$	$-1.95 \times 10^{-1}$
6	$2.13 \times 10^{-3}$	$5.92 \times 10^{-1}$	$-3.37 \times 10^{-1}$	$-2.54 \times 10^{-1}$
7	$2.82 \times 10^{-4}$	$8.00 \times 10^{-1}$	$-6.46 \times 10^{-1}$	$-2.08 \times 10^{-1}$
8	$-2.22 \times 10^{-3}$	1.04	-1.09	$-3.14 \times 10^{-2}$
9	$-6.60 \times 10^{-3}$	1.33	-1.81	$4.81 \times 10^{-1}$
10	$-1.22 \times 10^{-2}$	1.66	-2.73	1.25